PHYSICAL REVIEW B **79**, 144416 (2009)

Spin waves in a triangular lattice antiferromagnet: Decays, spectrum renormalization, and singularities

A. L. Chernyshev
Department of Physics, University of California, Irvine, California 92697, USA
and Max-Planck-Institut für Physik komplexer Systeme, 01187 Dresden, Germany

M. E. Zhitomirsky
Commissariat à l'Energie Atomique, DSM/INAC/SPSMS, F-38054 Grenoble, France
(Received 28 January 2009; published 15 April 2009)

We present a comprehensive study of the dynamical properties of the quantum Heisenberg antiferromagnet on a triangular lattice within the framework of spin-wave theory. The distinct features of spin-wave excitations in the triangular lattice antiferromagnet are (i) finite lifetime at zero temperature due to spontaneous two-magnon decays, (ii) strong renormalization of magnon energies $\varepsilon_{\mathbf{k}}$ with respect to the harmonic result, and (iii) logarithmic singularities in the decay rate $\Gamma_{\mathbf{k}}$. Quantum corrections to the magnon spectrum are obtained using both the on-shell and off-shell solutions of the Dyson equation with the lowest-order magnon self-energy. At low-energies magnon excitations remain well defined albeit with the anomalous decay rate $\Gamma_{\mathbf{k}} \propto k^2$ at $\mathbf{k} \to 0$ and $\Gamma_{\mathbf{k}} \propto |\mathbf{k}-\mathbf{Q}_{\mathrm{AF}}|^{7/2}$ at $\mathbf{k} \to \mathbf{Q}_{\mathrm{AF}}$. At high energies, magnons are heavily damped with the decay rate reaching $(2\Gamma_{\mathbf{k}}/\varepsilon_{\mathbf{k}}) \sim 0.3$ for the case $S=1/2$. The on-shell solution shows logarithmic singularities in $\Gamma_{\mathbf{k}}$ with the concomitant jumplike discontinuities in $\mathrm{Re}[\varepsilon_{\mathbf{k}}]$ along certain contours in the momentum space. Such singularities are even more prominent in the magnon spectral function $A(\mathbf{k},\omega)$. Although the off-shell solution removes such log singularities, the decay rates remain strongly enhanced. We also discuss the role of higher-order corrections and show that such singularities may lead to complete disappearance of the spectrum in the vicinity of certain $\mathbf{k}$ points. The kinematic conditions for two-magnon decays are analyzed for various generalizations of the triangular lattice antiferromagnet as well as for the *XXZ* model on a kagomé lattice. Our results suggest that decays and singularities in the spin-wave spectra must be ubiquitous in all these systems. In addition, we give a detailed introduction in the spin-wave formalism for noncollinear Heisenberg antiferromagnets and calculate several quantities for the triangular lattice model including the ground-state energy and the sublattice magnetization.

DOI: 10.1103/PhysRevB.79.144416 PACS number(s): 75.10.Jm, 75.30.Ds, 78.70.Nx

I. INTRODUCTION

Heisenberg antiferromagnet (HAF) on a triangular lattice has been a focus of much attention as one of the basic model systems in which geometric frustration and low dimensionality are expected to yield new physical phenomena. Although available experimental realizations of the triangular lattice antiferromagnet[1–6] are described by such a model only approximately, either due to anisotropies or because of additional interactions, the ideal nearest-neighbor Heisenberg antiferromagnet on a triangular lattice given by

$$\hat{\mathcal{H}} = J \sum_{\langle ij \rangle} \mathbf{S}_i \cdot \mathbf{S}_j \tag{1}$$

remains the principal reference point.

The semiclassical $S \gg 1$ triangular lattice HAF orders in the so-called 120° structure (see Fig. 1). Historically, it was anticipated that enhanced quantum fluctuations destroy the long-range antiferromagnetic order for the spin-1/2 model.[7] However, calculations of quantum corrections within the spin-wave theory have suggested that the 120° magnetic structure remains stable even for $S=1/2$.[8–11] The early numerical results for small clusters were less conclusive; some supporting magnetically disordered state[12] and some confirming the spin-wave results.[13] Since the quantum Monte Carlo suffers from the infamous sign problem when applied to frustrated models, it is not until the Green's function Monte Carlo work[14] that the magnetically ordered ground state of the spin-1/2 triangular lattice HAF has been generally agreed upon. More recent series-expansion[15] and density-matrix renormalization group (DMRG) studies[16] have confirmed the stability of the 120° spin structure for the case of $S=1/2$ and yielded the value of ordered moments $\langle S \rangle \approx 0.20$, close to the previous result.[14]

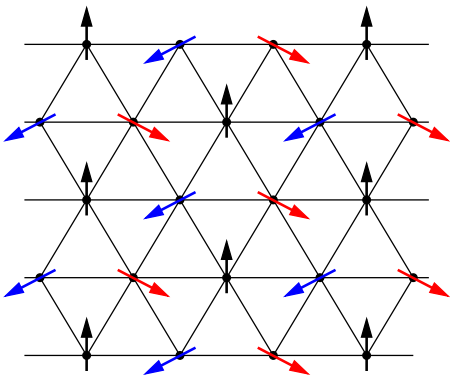

FIG. 1. (Color online) The ordered 120° spin structure of the triangular lattice HAF.

Gradually, it has been recognized that the truly distinct physics of the quantum triangular lattice antiferromagnet concerns its excitation spectrum and the thermodynamic properties. The anomalous behavior of the latter has been discovered earlier by the high-temperature series-expansion study.[17] The temperature dependence of such quantities as entropy or susceptibility exhibits significant differences between the triangular- and the square-lattice models: upon lowering temperature down to about $J/2$ the square-lattice antiferromagnet shows strong signs of ordering, while the triangular lattice one does not. More recently, developments in the series-expansion method have allowed to calculate the excitation spectra of the noncollinear spin systems directly.[15,18] Numerical results for the magnon band of the spin-1/2 triangular lattice HAF deviate substantially from the linear spin-wave theory (LSWT), with the overall band narrowing by $\sim 50\%$, flattening at the top of the spectrum, and extra "rotonlike" minima appearing at some special $\mathbf{k}$ points. These results are so different from the well-known square-lattice case, where the spectrum is renormalized only modestly and almost uniformly upward, that Ref. 18 suggested that at high energies the elementary excitations are not spin waves but spinons. This hypothesis was questioned by the subsequent studies which have looked into the role of magnon interactions within the framework of the spin-wave theory.[19,20] It was shown that the first-order $1/S$ correction strongly modifies the LSWT spectrum in an overall qualitative agreement with the series-expansion data. Further detailed comparison of the series-expansion and the spin-wave spectra has confirmed their qualitative similarities and outlined remaining differences.[15]

Simply by the virtue of observing such significant differences in the triangular- and square-lattice spectra, these works have explained the contrast in the thermodynamic behavior of the two systems. Since the spin-wave bandwidth of the triangular lattice HAF is reduced to $W \approx J$ and the other features such as the rotonlike minimum are at the energies $\approx J/2$,[15] the thermodynamic quantities must be dominated by these short-wavelength features down to much lower temperatures than in the square lattice case where the bandwidth is $W \approx 2J$ and the spectrum has a rather benign shape.

In the recent Letter[20] we have focused on another distinct feature of the spin-wave spectrum in the triangular lattice antiferromagnet: intrinsic damping due to spontaneous decays. Note that although the spectrum renormalization in the triangular lattice HAF is significant, the truly dramatic *qualitative* difference from the square-lattice case is the finite lifetime of the excitations at $T=0$. Aside from yielding a substantial damping for excitations in the most of the Brillouin zone, the first $1/S$ correction produces the logarithmic singularity in the imaginary part of $\varepsilon_{\mathbf{k}}$ accompanied by the jumps in the real part along some contours in the $\mathbf{k}$ space. We have analyzed the origin of such singularities and have related them to the topological transitions in the decay surfaces of magnons, which are due to the saddle-point van Hove singularities in the two-magnon continuum. Whether such logarithmic singularities are the artifact of the $1/S$ approximation of the theory or are the true features of the spectrum was only partially addressed in our work.[20] For the decays into magnons that themselves acquire finite lifetimes, singularity will disappear in the higher $1/S$ order and thus is not "real." However, if the singularity is due to decays into stable excitations, we concluded that the singularity remains essential and the magnon damping should remain very strong.[20]

We would like to mention that the numerical study did not observe jumps in the real part of the spectrum nor it reported the damping.[15] This can be used as an argument against any "physical" singularities. However, by design, the series-expansion method finds the spectrum that is purely real. Even with such restrictions, there where certain $\mathbf{k}$ points for which the numerically obtained $\varepsilon_{\mathbf{k}}$ had a convergence problem, shown by large error bars in Ref. 15.

Altogether, the qualitative questions remain: why there is such a substantial difference of the excitation spectrum in the triangular lattice HAF from the more conventional square-lattice case? How generic are the decays, singularities, and anomalously large role of spin-wave interactions? What happens to the spectrum near the singular points? It is the purpose of the present work to address these questions. First, we would like to provide a consistent overview of the spin-wave formalism as applied to the triangular lattice model in order to demonstrate the origin of the drastic differences between the spectra of the collinear and noncollinear ordered magnets. Second, we will elaborate on our previous findings on magnon decays and demonstrate that they must exist in a wide variety of frustrated spin models. Finally, we would like to extend our study beyond the on-shell approximation of the previous works and clarify the fate of the singularities in the spectrum.

The rest of the paper is organized as follows. Section II provides a qualitative discussion of the origin of the spectrum anomalies in the triangular lattice HAF and suggests a broader framework for the subsequent results. Section III gives a detailed description of the spin-wave formalism for a noncollinear HAF. Here, we also address the controversy over two different results for the $O(1/S^2)$ correction to the sublattice magnetization of the triangular lattice HAF, which exist in literature.[10,11] The first-order $O(1/S)$ quantum corrections for the spin-wave spectrum are considered in Sec. IV. Here we discuss the characteristic long-wavelength and short-wavelength features of both the spectrum renormalization and the decay rates. In Sec. V, we discuss in detail the kinematic decay conditions for a generic single-particle spectrum coupled to the two-particle continuum. The relation between the singularities in the renormalized spectrum and the topological transitions in the decay surfaces is established in this section. Section VI is devoted to the discussion of the off-shell solution of the Dyson equation in the complex plane. We show that in the strong-coupling regime, the solution may cease to exist and the magnon pole may disappear in the vicinity of the logarithmic singularity. The results of the numerical off-shell solution of the Dyson equation for the triangular lattice HAF are presented and it is shown that the damping remains very substantial. In this section we also present the results for the spectral function for several representative $\mathbf{k}$ points and the quasiparticle residues across the Brillouin zone. We show that the log singularities become even more prominent in the spectral functions, complicating the conventional analysis. In Sec. VII we discuss several examples of other models in which decays and singularities

are ubiquitous, such as the easy-plane *XXZ* and orthorhombically distorted $J-J'$ models on a triangular lattice as well as the *XXZ* model on a kagomé lattice. Section VIII contains final conclusions and Appendixes A–E are used to provide more technical details.

II. QUALITATIVE DISCUSSION

A. Cubic anharmonicities

In the case of quantum Heisenberg antiferromagnets on bipartite lattices in $D \geq 2$, the spin-wave theory agrees extremely well with the available numerical data, even for the "most quantum" spin-1/2 square-lattice model.[21–24] Therefore, not only one needs to understand the apparent anomalies found for the Heisenberg antiferromagnet on a triangular lattice, but also to explain why such anomalies are not present in the properties of the same model on bipartite lattices. In the following we give qualitative arguments that the unusual behavior stems from noncollinearity of spins in the ordered state, which is, in turn, induced by geometrical frustration.

In quantum magnets with *collinear* spin configurations, the interaction between spin-wave excitations is described by quartic and higher-order anharmonicities.[25–27] In contrast, a general quantum system with nonconserved number of particles is *expected* to have anharmonicities of all orders beginning with cubic terms, which describe interaction between one- and two-particle states. The common examples are phonons in crystals[28] and excitations in superfluid bosonic systems.[29] In quantum spin liquids, such as spin ladders and various dimer systems, triplet excitations may also have three-particle interaction terms.[30,31]

For the ordered spin systems, cubic anharmonicities correspond to coupling of the transverse (one-magnon) and longitudinal (two-magnon) fluctuations, which would require the presence of mixing terms between S^z and $S^{x,y}$ spin components. Such terms are absent in the collinear Heisenberg magnets due to remaining $U(1)$ rotational symmetry about the direction of the magnetic order parameter. On the other hand, in the *noncollinear* antiferromagnets spin canting produces coupling of the transverse fluctuations in one sublattice to the longitudinal ones in the others. As a result, this yields cubic terms in the magnon-magnon interaction.[10,11,32–35]

Noncollinear spin configurations in the Heisenberg antiferromagnets can be induced either by an external magnetic field or by frustrating interactions. In the former case, spin canting and cubic anharmonicities are small in weak fields. At higher fields, cubic interactions dominate and lead to spontaneous magnon decays above threshold field H^*.[36–38] In frustrated magnets, spin canting and cubic terms are substantial already in zero field and thus play the key role in the spectrum renormalization.

The above discussion creates a broader view on the ordered quantum magnets and their spectra. Magnets with collinear spin structures have excitations that are intrinsically weakly coupled. Not only the energy is minimized by the collinear spin orientation, but the interactions are also weak. Having a noncollinear spin structure necessarily implies much stronger coupling among the excitations. Thus, the collinear antiferromagnets should be considered if not as an exception, but at least as a simplified subclass of quantum antiferromagnets. Naturally, many of their properties that are commonly assumed to be valid for all ordered antiferromagnets, such as the ubiquitously close agreement of the harmonic theory with numerical results, should not be expected to hold in general.

Somewhat more formally, the lack of cubic anharmonicities in collinear spin systems results in the absence of certain class of diagrams in the perturbative expansion. In the first order in $1/S$, the only nonvanishing contribution is given by simple "balloon" Hartree-Fock-type terms (see Fig. 3). Since these are ω independent, the corresponding correction to the spin-wave energy is a trivial redefinition of the interaction strength. The first ω-dependent correction appears only in the second order in $1/S$ and is already quite weak due to small phase-space factor. In noncollinear spin systems, cubic anharmonicity generates "bubble" diagrams already in the lowest $1/S$ order, not only inducing a substantial spectrum correction but also providing a channel for the decays if the decay conditions are fulfilled. In the triangular lattice HAF both effects are amplified because of the lower dimensionality and because the tilting angle between spins is not small. Hence, the strong coupling of the longitudinal and transverse modes in noncollinear magnets in general and in the triangular lattice HAF in particular is the key to understanding strong renormalization of their spectra from the results of the harmonic approximation.

B. Decays and singularities

Another important property of noncollinear magnets is the ubiquitous propensity of the excitations to spontaneous decays. The presence of transverse-to-longitudinal coupling is a necessary but not a sufficient condition for decays. In addition, the energy and momentum must be conserved in the decay process, yielding kinematic restrictions. Decays depend, therefore, on the *shape* of the single-particle dispersion that may, or may not, allow for spontaneous decays. While we will give a detailed classification of various kinematic conditions later (see Sec. V), there are simple arguments for the decays to exist in the triangular lattice HAF. The complete breaking of the $SO(3)$ rotational symmetry by the 120° spin structure leads to three Goldstone modes:[39] one at the center of the Brillouin zone and two at the ordering vectors $\pm\mathbf{Q}$. The former mode can be related to an infinitesimal twist of spins about the axis which is perpendicular to the spin plane, while the other two correspond to twists about the axes lying in the spin plane. The velocity of the latter modes is smaller than that of the former one. Such a difference guarantees that the energy conservation can always be satisfied for the decay of the fast quasiparticle into a pair of slower magnons, similar to the decay of the longitudinal phonon into a pair of the transverse ones in crystals.[28] Since cubic anharmonicities necessarily generate couplings between all magnon branches, this ensures finite lifetime for spin excitations in an extended part of the Brillouin zone at $T=0$. The above consideration is trivially generalized to

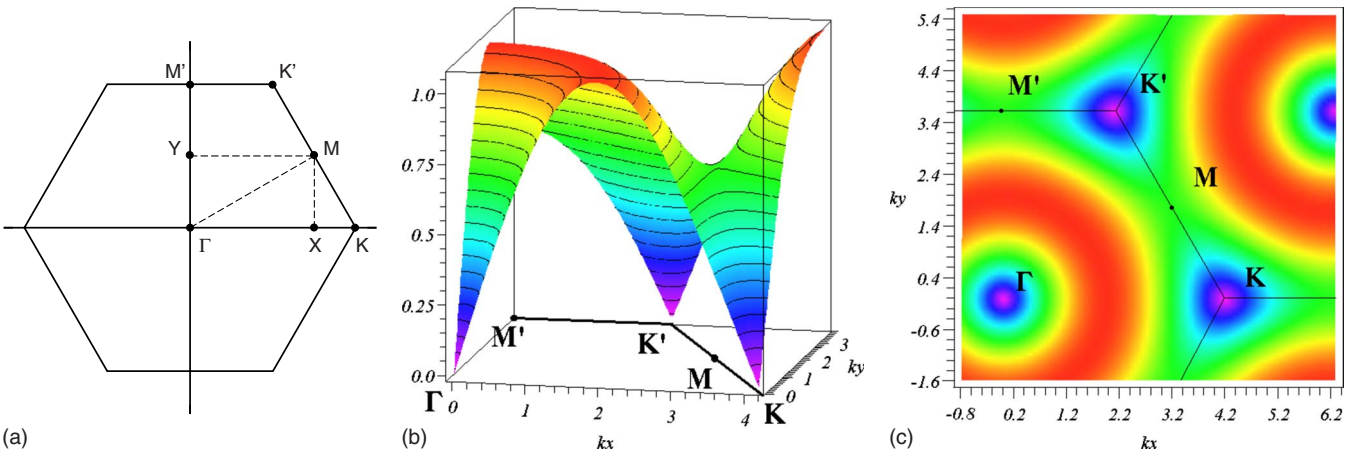

FIG. 2. (Color online) Left panel: the Brillouin zone of a triangular lattice, lines are representative cuts. Central panel: 3D plot of the linear spin-wave energy $\omega_{\mathbf{k}}$ in the triangular lattice HAF. Right panel: intensity plot of $\omega_{\mathbf{k}}$. Note different velocities of the Goldstone modes and different symmetries of the dispersion near Γ and K (K') points and the saddle point at M (M').

other frustrated antiferromagnets where symmetry guarantees existence of more than one type of the Goldstone mode. We will elaborate on the decays in the *XXZ* anisotropic and orthorhombically distorted triangular lattice antiferromagnets (AFs) as well as on the kagomé AF in Sec. VII. We would like to note that the kinematic conditions for decays can be completely suppressed by magnetic anisotropies, still leaving spins in a noncollinear configuration. In that case decays are absent but the renormalization of the real part of the spectrum due to spin-wave interaction remains substantial.

In the following, we also discuss extensively the singularities that occur in the decay rates of single-particle spectra due to the van Hove singularities in the two-particle continuum. While the main conclusion is that the essential singularities are cut off either by the finite lifetime of the decay products or by the nonsingular finite lifetime of the decaying particle, the decay rates remain parametrically enhanced by such singularities. A qualitative estimate of such a singularity-enhanced decay rate in the two-dimensional case is

$$\Gamma_{\mathbf{k}} \simeq (V_3^2/S)\ln(\Lambda S/V_3^2), \tag{2}$$

where V_3 is the strength of a three-particle decay vertex and Λ is the momentum cutoff. Even for large values of spin S the decay rate $\Gamma_{\mathbf{k}}$ is logarithmically enhanced relative to a perturbative result $\Gamma_{\mathbf{k}} \sim 1/S$.

III. SPIN-WAVE FORMALISM

A. Bosonic Hamiltonian

The spin-wave theory of collinear antiferromagnets on bipartite lattices is commonly formulated by introducing bosonic operators according to the number of magnetic sublattices.[26,27] In the Heisenberg triangular lattice antiferromagnet spins form the three-sublattice 120° structure at $T=0$ (see Fig. 1). In order to go beyond the linear spin-wave analysis,[8,9] it is convenient to transform to a rotating frame with the z axis pointing along the local spin direction. Then, one needs to define only single species of boson operators with the wave vectors that belong to the full paramagnetic Brillouin zone (BZ) (Fig. 2). We would like to note that even in collinear antiferromagnets the above approach has substantial advantage when calculating higher-order spin-wave corrections. Furthermore, such a "single-sublattice" procedure has no alternatives when considering generic, incommensurate (spiral-like) antiferromagnetic ordering.

As a first step, we assume that spins lie in the x-z plane and perform transformation from the laboratory frame (x_0, z_0) into the rotating frame (x, z),

$$S_i^{z_0} = S_i^z \cos\,\theta_i - S_i^x \sin\,\theta_i,$$

$$S_i^{x_0} = S_i^z \sin\,\theta_i + S_i^x \cos\,\theta_i, \tag{3}$$

where $\theta_i = \mathbf{Q}\cdot\mathbf{r}_i$ and $\mathbf{Q} = (4\pi/3, 0)$ is the ordering wave vector of the 120° spin structure. The spin Hamiltonian, Eq. (1), in the new coordinate system takes the following form:

$$\hat{\mathcal{H}} = J\sum_{\langle ij\rangle} [S_i^y S_j^y + \cos(\theta_i - \theta_j)(S_i^z S_j^z + S_i^x S_j^x)$$
$$+ \sin(\theta_i - \theta_j)(S_i^z S_j^x - S_i^x S_j^z)], \tag{4}$$

where $\langle ij\rangle$ denotes, as usual, summation over the nearest-neighbor bonds.

The bosonization of Eq. (4) is performed via the Hermitian Holstein-Primakoff transformation

$$S_i^z = S - a_i^\dagger a_i, S_i^- = a^\dagger\sqrt{2S - a_i^\dagger a_i}, \tag{5}$$

where $S_i^\pm = S_i^x \pm i S_i^y$ with subsequent expansion of square roots to the first order in $a_i^\dagger a_i/2S$. Such an approximation is sufficient to calculate the $O(1/S^2)$ corrections to the ground-state energy and to the sublattice magnetization and to determine the $O(1/S)$ correction to the spin-wave dispersion. The resultant spin-wave Hamiltonian is given by

$$\hat{\mathcal{H}}_{\mathrm{SW}} = \hat{\mathcal{H}}_0 + \hat{\mathcal{H}}_2 + \hat{\mathcal{H}}_3 + \hat{\mathcal{H}}_4 + O(S^{-1}), \tag{6}$$

where $\hat{\mathcal{H}}_n$ denote terms of the nth power in the original (Holstein-Primakoff) boson operators $a_i^\dagger$ and a_i. The first

term in this expansion is the classical energy $\hat{\mathcal{H}}_0=-\frac{3}{2}JS^2N$. Terms that are linear in a_i and $a_i^\dagger$ vanish automatically because the 120° spin structure corresponds to a minimum of the classical energy. Note that the Hamiltonian (6) also yields a series in powers of S, with $\hat{\mathcal{H}}_0=O(S^2)$, $\hat{\mathcal{H}}_2=O(S^1)$, $\hat{\mathcal{H}}_3=O(S^{1/2})$, and $\hat{\mathcal{H}}_4=O(S^0)$, respectively. The subsequent treatment of $\hat{\mathcal{H}}_{\rm SW}$ consists of diagonalizing the harmonic part $\hat{\mathcal{H}}_2$ exactly and, then, treating $\hat{\mathcal{H}}_3$ and $\hat{\mathcal{H}}_4$ as perturbations.

1. Linear spin-wave theory

Noninteracting magnons are described by the LSWT or the harmonic approximation. After the Fourier transformation, the quadratic part of $\hat{\mathcal{H}}_{\rm SW}$ reads

$$\hat{\mathcal{H}}_2=\sum_{\mathbf{k}}\left[A_{\mathbf{k}}a_{\mathbf{k}}^\dagger a_{\mathbf{k}}-\frac{1}{2}B_{\mathbf{k}}(a_{\mathbf{k}}^\dagger a_{-\mathbf{k}}^\dagger+a_{-\mathbf{k}}a_{\mathbf{k}})\right],$$

$$A_{\mathbf{k}}=3JS\left(1+\frac{1}{2}\gamma_{\mathbf{k}}\right),\quad B_{\mathbf{k}}=\frac{9}{2}JS\gamma_{\mathbf{k}},\tag{7}$$

where $\gamma_{\mathbf{k}}$ is a sum over the nearest-neighbor sites

$$\gamma_{\mathbf{k}}=\frac{1}{6}\sum_{\boldsymbol{\delta}}e^{i\mathbf{k}\boldsymbol{\delta}}=\frac{1}{3}\left(\cos k_x+2\cos\frac{k_x}{2}\cos\frac{\sqrt{3}}{2}k_y\right).\tag{8}$$

Diagonalization of $\hat{\mathcal{H}}_2$ is performed with the help of the canonical Bogolyubov transformation

$$a_{\mathbf{k}}=u_{\mathbf{k}}b_{\mathbf{k}}+v_{\mathbf{k}}b_{-\mathbf{k}}^\dagger\tag{9}$$

under conditions $u_{\mathbf{k}}^2-v_{\mathbf{k}}^2=1$ and

$$u_{\mathbf{k}}^2+v_{\mathbf{k}}^2=\frac{A_{\mathbf{k}}}{\sqrt{A_{\mathbf{k}}^2-B_{\mathbf{k}}^2}},\quad 2u_{\mathbf{k}}v_{\mathbf{k}}=\frac{B_{\mathbf{k}}}{\sqrt{A_{\mathbf{k}}^2-B_{\mathbf{k}}^2}}.\tag{10}$$

As a result, the linear spin-wave Hamiltonian takes the following form:

$$\hat{\mathcal{H}}_0+\hat{\mathcal{H}}_2=-\frac{3}{2}JS(S+1)N+\sum_{\mathbf{k}}\varepsilon_{\mathbf{k}}\left(b_{\mathbf{k}}^\dagger b_{\mathbf{k}}+\frac{1}{2}\right).\tag{11}$$

In the harmonic approximation, spin waves are noninteracting bosons with the energy

$$\varepsilon_{\mathbf{k}}=\sqrt{A_{\mathbf{k}}^2-B_{\mathbf{k}}^2}=3JS\omega_{\mathbf{k}},\tag{12}$$

where we define the dimensionless frequency

$$\omega_{\mathbf{k}}=\sqrt{(1-\gamma_{\mathbf{k}})(1+2\gamma_{\mathbf{k}})}.\tag{13}$$

The shape of $\omega_{\mathbf{k}}$ is shown in Fig. 2. The harmonic spectrum of the triangular lattice HAF has several distinct features. The intensity map clearly shows that the velocities of the Goldstone modes at Γ ($\mathbf{k}=0$) and K, K' ($\mathbf{k}=\pm\mathbf{Q}$) points are different. They are given by

$$v_0^{(0)}=3JS\frac{\sqrt{3}}{2},\quad v_Q^{(0)}=3JS\sqrt{\frac{3}{8}}.\tag{14}$$

Another notable feature is the clear threefold symmetry of the modes near $\mathbf{Q}$ points. Instead of the usual convex and isotropic form, the spin-wave energy at small $\tilde{\mathbf{k}}=\mathbf{k}-\mathbf{Q}$ is nonanalytic with varying convexity

$$\varepsilon_{\mathbf{k}}\approx v_Q\tilde{k}(1-\alpha_\varphi\tilde{k}),\quad \text{where}\quad \alpha_\varphi\sim\cos 3\varphi.\tag{15}$$

The overall shape of the dispersion is also more complicated than in the square-lattice antiferromagnet. At the M point, the center of the BZ edge, $\omega_{\mathbf{k}}$ has a saddle point with the energy roughly half of the bandwidth. Thus, already with the harmonic spectrum the thermodynamic response at intermediate temperatures should be quite different from that in the square-lattice antiferromagnet.

We introduce now several nonzero Hartree-Fock averages that contribute to the spin-wave corrections of many static and dynamic quantities of the triangular lattice HAF

$$n=\langle a_i^\dagger a_i\rangle,\quad m=\langle a_i^\dagger a_j\rangle,\quad \Delta=\langle a_i a_j\rangle,\quad \delta=\langle a_i^2\rangle.\tag{16}$$

In the harmonic theory these are expressed as linear combinations of the two-dimensional (2D) integrals

$$c_l=\sum_{\mathbf{k}}\frac{(\gamma_{\mathbf{k}})^l}{\omega_{\mathbf{k}}},\tag{17}$$

with $l=0,1,2$ (see Appendix A for further details). In particular, the linear spin-wave correction to the staggered magnetization, $\langle S\rangle=S-\delta S$, is given by

$$\delta S\equiv n=\frac{1}{4}(2c_0-2+c_1)=0.261\ 303\ 2.\tag{18}$$

2. Spin-wave interaction: Cubic terms

The cubic interaction terms $\hat{\mathcal{H}}_3$ in Eq. (6) have no analog in collinear magnets. They originate from the coupling of local S^z and S^x spin components in Eq. (4). In terms of the original boson operators (5) the cubic interaction is given by

$$\hat{\mathcal{H}}_3=J\sqrt{\frac{S}{2}}\sum_{\langle ij\rangle}\sin(\theta_j-\theta_i)[a_i^\dagger a_i(a_j^\dagger+a_j)-a_j^\dagger a_j(a_i^\dagger+a_i)].\tag{19}$$

For the collinear spin structures, $\sin(\theta_j-\theta_i)\equiv 0$ and the cubic terms vanish identically.

Performing consecutively the Fourier and Bogolyubov transformations from $a_i^\dagger$, a_i to $b_{\mathbf{k}}^\dagger$, $b_{\mathbf{k}}$ operators in $\hat{\mathcal{H}}_3$ we obtain the interaction terms expressed via the "new" bosons

$$\hat{\mathcal{H}}_3=\sum_{\mathbf{k},\mathbf{q}}\left[\frac{1}{2!}\Gamma_1(\mathbf{q},\mathbf{k}-\mathbf{q};\mathbf{k})b_{\mathbf{q}}^\dagger b_{\mathbf{k}-\mathbf{q}}^\dagger b_{\mathbf{k}}+\frac{1}{3!}\Gamma_2(\mathbf{q},-\mathbf{k}-\mathbf{q},\mathbf{k})b_{\mathbf{q}}^\dagger b_{-\mathbf{k}-\mathbf{q}}^\dagger b_{\mathbf{k}}^\dagger+\text{H.c.}\right].\tag{20}$$

Generally, terms linear in $b_{\mathbf{Q}}^\dagger$ and $b_{\mathbf{Q}}$ also appear after the above substitution. They represent quantum correction to the pitch angle of the spin helix[33,40,41] or to the spin canting angle in an external magnetic field.[34,36,42] Such a correction vanishes in the triangular lattice HAF because the ordering wave vector $\mathbf{Q}$ corresponds to a stable symmetry point in BZ.

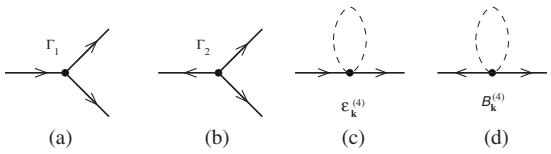

FIG. 3. The lowest-order vertices that yield $1/S$ corrections to the spectrum and $1/S^2$ contributions to the static properties.

The first term in Eq. (20) describes interaction between one- and two-magnon states and is symmetric under permutation of two outgoing momenta. We call it the "decay" term, although the decay processes may be only virtual. The second term in Eq. (20) corresponds to the spontaneous creation of three magnons and we refer to it as to the "source" term. The source vertex is symmetric under permutation of all three momenta. Making the energy and spin dependences of the three-boson interactions explicit, we define dimensionless vertices related to the original ones (20) by

$$\Gamma_{1,2}(1,2;3) = 3iJ\sqrt{\frac{3S}{2}}\tilde{\Gamma}_{1,2}(1,2;3), \tag{21}$$

with $\tilde{\Gamma}_{1,2}$ given by

$$\tilde{\Gamma}_1(1,2;3) = \bar{\gamma}_1(u_1+v_1)(u_2u_3+v_2v_3) + \bar{\gamma}_2(u_2+v_2)(u_1u_3 + v_1v_3) - \bar{\gamma}_3(u_3+v_3)(u_1v_2+v_1u_2),$$

$$\tilde{\Gamma}_2(1,2;3) = \bar{\gamma}_1(u_1+v_1)(u_2v_3+v_2u_3) + \bar{\gamma}_2(u_2+v_2)(u_1v_3 + v_1u_3) + \bar{\gamma}_3(u_3+v_3)(u_1v_2+v_1u_2), \tag{22}$$

where u_i, v_i are the Bogolyubov parameters (10) and the function $\bar{\gamma}_{\mathbf{k}}$ is defined as

$$\bar{\gamma}_{\mathbf{k}} = \frac{1}{3}\left(\sin k_x - 2\sin\frac{k_x}{2}\cos\frac{\sqrt{3}}{2}k_y\right). \tag{23}$$

The diagrammatic representations of the decay and the source vertices are shown in Figs. 3(a) and 3(b), respectively. The above form of $\Gamma_{1,2}$ coincides with the expressions used by Miyake.[10,32]

3. Spin-wave interaction: Quartic terms

The last term in the spin-wave Hamiltonian (6) represents the quartic terms

$$\hat{\mathcal{H}}_4 = \frac{J}{4}\sum_{\langle ij\rangle}\left[-a_i^\dagger a_i a_j^\dagger a_j + \frac{3}{4}(a_i^\dagger a_i a_i a_j + a_j^\dagger a_j a_j a_i) - \frac{1}{4}(a_j^\dagger a_i^\dagger a_i a_i + a_j^\dagger a_j^\dagger a_j a_i)\right] + \text{H.c.} \tag{24}$$

After the Bogolyubov transformation and normal ordering of b operators, the interaction (24) is replaced with

$$\hat{\mathcal{H}}_4 = \delta E_4 + \delta\tilde{H}_2 + \tilde{H}_4, \tag{25}$$

where the first two terms are the Hartree-Fock corrections to the ground-state energy and to the magnon self energy, Figs. 3(c) and 3(d), respectively. The magnon self-energy $\delta\tilde{H}_2$ contains both the diagonal and the off-diagonal terms, while for the square-lattice HAF the anomalous off-diagonal terms vanish. The final term $\tilde{H}_4$ describes two-particle scattering processes. Similar to the case of the collinear antiferromagnets,[27] this latter term yields only higher-order $1/S$ corrections compared to δE_4 and $\delta\tilde{H}_2$ and is, therefore, neglected in the present work.

To derive the explicit form of Eq. (25), it is technically more straightforward to apply the Hartree-Fock decouplings (16) to Eq. (24) and use the Bogolyubov transformation in $\delta\tilde{H}_2$ afterward. This is analogous to the treatment of quartic terms for collinear antiferromagnets.[26] With the details of this derivation delineated in Appendix A, we simply list the end result for the correction to the ground-state energy

$$\delta E_4 = -\frac{3}{8}J\left[(c_0+c_1-2c_2-1)^2 - \frac{3}{2}(c_1-c_2)^2\right] \tag{26}$$

and to the harmonic spin-wave Hamiltonian

$$\delta\tilde{\mathcal{H}}_2 = \sum_{\mathbf{k}}\varepsilon_{\mathbf{k}}^{(4)}b_{\mathbf{k}}^\dagger b_{\mathbf{k}} - \frac{1}{2}B_{\mathbf{k}}^{(4)}(b_{\mathbf{k}}b_{-\mathbf{k}} + b_{-\mathbf{k}}^\dagger b_{\mathbf{k}}^\dagger), \tag{27}$$

where the first-order magnon energy correction and the anomalous self-energy terms are expressed as

$$\varepsilon_{\mathbf{k}}^{(4)} = \frac{3J}{4\omega_{\mathbf{k}}}[\gamma_{\mathbf{k}}^2(4c_0+c_1-5c_2-4) + \gamma_{\mathbf{k}}(2-2c_0+c_1+c_2) - 2c_0-2c_1+4c_2+2] \tag{28}$$

and

$$B_{\mathbf{k}}^{(4)} = -\frac{9J}{8\omega_{\mathbf{k}}}(1-\gamma_{\mathbf{k}})(c_1+2c_2\gamma_{\mathbf{k}}), \tag{29}$$

respectively.

4. Effective Hamiltonian

With the triangular lattice model discussed in detail, we would like to outline the structure of the spin-wave Hamiltonian for a generic noncollinear spin system. After the Holstein-Primakoff and Bogolyubov transformations with subsequent renormalization, when necessary, of the classical configuration, the spin-wave Hamiltonian takes the form of a polynomial of terms with increasing number of bosons, $\tilde{\mathcal{H}}_0+\tilde{\mathcal{H}}_2+\tilde{\mathcal{H}}_3+\ldots$, and decreasing power of S. Therefore, the spin-wave expansion to order $O(S^0)$ will always result in an effective Hamiltonian

$$\tilde{\mathcal{H}}_{\text{eff}} = \sum_{\mathbf{k}}[\tilde{\varepsilon}_{\mathbf{k}}b_{\mathbf{k}}^\dagger b_{\mathbf{k}} + V_{\mathbf{k}}^{od}(b_{\mathbf{k}}b_{-\mathbf{k}} + b_{-\mathbf{k}}^\dagger b_{\mathbf{k}}^\dagger)] + \sum_{\mathbf{k},\mathbf{q}}[V_{\mathbf{k},\mathbf{q}}b_{\mathbf{q}}^\dagger b_{\mathbf{k}-\mathbf{q}}^\dagger b_{\mathbf{k}} + F_{\mathbf{k},\mathbf{q}}b_{\mathbf{q}}^\dagger b_{-\mathbf{k}-\mathbf{q}}^\dagger b_{\mathbf{k}}^\dagger + \text{H.c.}]. \tag{30}$$

The spin-wave Hamiltonian for a *collinear* antiferromagnet is the restricted form of Eq. (30) with no three-boson terms present. The dynamic interaction among magnons in such a system occurs only in the next order due to the four-boson

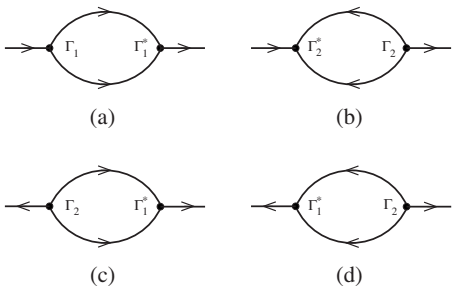

FIG. 4. The lowest order normal [(a) and (b)] and anomalous [(c) and (d)] magnon self-energies generated by cubic vertices.

terms that are substantially weaker. In addition, for the commonly studied case of the nearest-neighbor square- and cubic-lattice antiferromagnets, the anomalous quadratic terms in Eq. (30) also vanish, leaving only a benign energy renormalization. Altogether, the role of magnon interactions in collinear spin states is significantly less important than for noncollinear ones.

The effective Hamiltonian (30) provides a basis for the systematic perturbative calculations of various properties of the triangular lattice HAF. Parameters of the Hamiltonian (30) for the triangular lattice case were derived in previous sections

$$\widetilde{\varepsilon}_{\mathbf{k}} = \varepsilon_{\mathbf{k}} + \varepsilon^{(4)}_{\mathbf{k}}, \quad V^{od}_{\mathbf{k}} = -\frac{1}{2} B^{(4)}_{\mathbf{k}},$$

$$V_{\mathbf{k},\mathbf{q}} = \frac{1}{2!}\Gamma_1(\mathbf{q},\mathbf{k}-\mathbf{q};\mathbf{k}), \quad F_{\mathbf{k},\mathbf{q}} = \frac{1}{3!}\Gamma_2(\mathbf{q},-\mathbf{k}-\mathbf{q},\mathbf{k}), \tag{31}$$

where $\varepsilon_{\mathbf{k}} \sim O(S^1)$, $\varepsilon^{(4)}_{\mathbf{k}}$ and $B^{(4)}_{\mathbf{k}} \sim O(S^0)$, and $\Gamma_{1,2} \sim O(S^{1/2})$.

Using the standard diagrammatic technique for bosons at zero temperature, we define the bare magnon propagator as

$$G_0^{-1}(\mathbf{k},\omega) = \omega - \varepsilon_{\mathbf{k}} + i0. \tag{32}$$

Then, the lowest-order diagrams contributing in the order $O(S^0)$ to the normal and anomalous self-energies are shown in Figs. 3(c), 3(d), and 4. The corresponding expressions for the normal self-energies are

$$\Sigma^{(a)}_{11}(\mathbf{k},\omega) = \frac{1}{2}\sum_{\mathbf{q}} \frac{|\Gamma_1(\mathbf{q};\mathbf{k})|^2}{\omega - \varepsilon_{\mathbf{q}} - \varepsilon_{\mathbf{k}-\mathbf{q}} + i0}, \tag{33}$$

$$\Sigma^{(b)}_{11}(\mathbf{k},\omega) = -\frac{1}{2}\sum_{\mathbf{q}} \frac{|\Gamma_2(\mathbf{q};\mathbf{k})|^2}{\omega + \varepsilon_{\mathbf{q}} + \varepsilon_{\mathbf{k}+\mathbf{q}} - i0}. \tag{34}$$

From now on we shall use, for brevity, only two momenta in the notations for the cubic vertices (22). The anomalous self-energies are calculated as

$$\Sigma^{(c)}_{12}(\mathbf{k},\omega) = -\frac{1}{2}\sum_{\mathbf{q}} \frac{\Gamma_2(\mathbf{q};\mathbf{k})\Gamma^*_1(\mathbf{q};-k)}{\omega + \varepsilon_{\mathbf{q}} + \varepsilon_{\mathbf{k}+\mathbf{q}} - i0}, \tag{35}$$

$$\Sigma^{(d)}_{12}(\mathbf{k},\omega) = \frac{1}{2}\sum_{\mathbf{q}} \frac{\Gamma_2(\mathbf{q};-\mathbf{k})\Gamma^*_1(\mathbf{q};\mathbf{k})}{\omega - \varepsilon_{\mathbf{q}} - \varepsilon_{\mathbf{k}-\mathbf{q}} + i0}. \tag{36}$$

Finally, the two frequency-independent contributions to the normal and anomalous self-energies are given directly by the Hartree-Fock terms

$$\Sigma^{\mathrm{HF}}_{11}(\mathbf{k}) = \varepsilon^{(4)}_{\mathbf{k}} \quad \text{and} \quad \Sigma^{\mathrm{HF}}_{12}(\mathbf{k}) = -B^{(4)}_{\mathbf{k}} \tag{37}$$

of Figs. 3(c) and 3(d), respectively. The structure of the lowest-order contributions (33)–(37) remains valid, with necessary modifications of vertices, for an arbitrary noncollinear antiferromagnet.

B. Static properties

Previous works on the spin-wave theory for the triangular lattice HAF have calculated the second-order $1/S$ corrections to the ground-state energy and to the sublattice magnetization. Two approaches have been employed for calculation of the latter: numerical extrapolation of the response to small staggered magnetic field[10] and a direct diagrammatic expansion.[11] Surprisingly, they have produced two different results: $\Delta S_2 = 0.011/(2S)$ versus $0.027/(2S)$, respectively. While the latter approach has to deal with more singular higher-dimensional integrals, the former one relies on numerical extrapolation in a small parameter. Below, we resolve the controversy over the value of the staggered magnetization in favor of the Miyake's result[10] by following the diagrammatic approach of Chubukov *et al.*[11] and pointing out a delicate issue with numerical evaluation of canceling singularities under integrals. For completeness we also briefly discuss the ground-state energy correction.

1. Ground-state energy

The first two terms in the $1/S$ expansion of the ground-state energy of the triangular lattice HAF are given by Eq. (11). Here, we calculate the next-order correction resulting from the magnon interactions. The contribution from the quartic terms has already been obtained in the course of deriving the spin-wave Hamiltonian and is given by Eq. (26). Another correction of the same order is generated by the source vertex [Fig. 3(b)]

$$\delta E_3 = -\frac{1}{3!}\sum_{\mathbf{k},\mathbf{q}} \frac{|\Gamma_2(\mathbf{q};\mathbf{k})|^2}{\varepsilon_{\mathbf{k}} + \varepsilon_{\mathbf{q}} + \varepsilon_{\mathbf{k}+\mathbf{q}}}. \tag{38}$$

Combining all these contributions together one finds in the second order in $1/S$,

$$E_{\mathrm{gs}}/N = -\frac{3}{2}JS^2\left[1 + \frac{I_2}{S} + \frac{(I_4 + 2I_3)}{(2S)^2}\right], \tag{39}$$

where $I_2 = (1 - \Sigma_{\mathbf{k}}\omega_{\mathbf{k}})$ and the constants I_4 and I_3 are straightforwardly related to δE_4,

$$I_4 = (c_0 + c_1 - 2c_2 - 1)^2 - \frac{3}{2}(c_1 - c_2)^2 \approx -0.254\,293, \tag{40}$$

and to δE_3,

$$I_3 = \sum_{\mathbf{k},\mathbf{q}} \frac{\tilde{\Gamma}_2(\mathbf{q},\mathbf{k})^2}{\omega_\mathbf{k} + \omega_\mathbf{q} + \omega_{\mathbf{k}+\mathbf{q}}} = 0.137\ 85(1). \tag{41}$$

The above four-dimensional integral has been calculated by two different methods: the Monte Carlo integration and the finite-size extrapolation of lattice sums using clusters with different aspect ratios,[16] both agreeing in all significant digits. Altogether, the ground-state energy in the second order of $1/S$ expansion is

$$E_{gs}/N = -\frac{3}{2}JS^2\left[1 + \frac{0.436\ 824}{2S} + \frac{0.021\ 41}{(2S)^2}\right]. \tag{42}$$

The above result agrees with the previous calculation[32] improving on the numerical accuracy of the last term.

2. Sublattice magnetization

To calculate the staggered magnetization we use the diagrammatic approach which is very close, aside from a few technical details, to the one used in Ref. 11. Within the spin-wave approach the sublattice magnetization is

$$\langle S\rangle = S - \langle a_i^\dagger a_i\rangle = S - \delta S, \tag{43}$$

where the quantum correction δS is expressed as

$$\delta S = \sum_\mathbf{k} [v_\mathbf{k}^2 + (u_\mathbf{k}^2 + v_\mathbf{k}^2)\langle b_\mathbf{k}^\dagger b_\mathbf{k}\rangle + 2u_\mathbf{k}v_\mathbf{k}\langle b_\mathbf{k} b_{-\mathbf{k}}\rangle]. \tag{44}$$

The first term under the sum is the LSWT result[8,9] already given by Eq. (18)

$$\delta S_1 = \sum_\mathbf{k} v_\mathbf{k}^2 \approx 0.261\ 303\ 2. \tag{45}$$

The two remaining terms in Eq. (44) contain bosonic averages which vanish in the linear spin-wave (LSW) approximation and contribute only to the next order in $1/S$. Therefore, we write

$$\langle S\rangle = S - \delta S_1 - \frac{\delta S_2}{2S}, \tag{46}$$

where the last correction has two contributions:

$$\frac{\delta S_2}{2S} = \delta S_{2,1} + \delta S_{2,2},$$

$$\delta S_{2,1} = \sum_\mathbf{k} \frac{1 + \frac{1}{2}\gamma_\mathbf{k}}{\omega_\mathbf{k}}\langle b_\mathbf{k}^\dagger b_\mathbf{k}\rangle, \quad \delta S_{2,2} = \frac{3}{2}\sum_\mathbf{k} \frac{\gamma_\mathbf{k}}{\omega_\mathbf{k}}\langle b_\mathbf{k} b_{-\mathbf{k}}\rangle. \tag{47}$$

Calculation of the bosonic averages in the above expression must be performed to the first order in $1/S$. As explained in Appendix B, these averages are straightforwardly related to the normal and anomalous self-energies (see Figs. 3 and 4). In particular, the magnon occupation number $\langle b_\mathbf{k}^\dagger b_\mathbf{k}\rangle$ is only due to $\Sigma_{11}^{(b)}$ from Fig. 4(b), while the other two normal self-energy corrections, $\Sigma_{11}^{(a)}$ and $\Sigma_{11}^{\mathrm{HF}}$, have zero contributions. On the other hand, all three off-diagonal self-energies, $\Sigma_{12}^{(c)}$, $\Sigma_{12}^{(d)}$, and $\Sigma_{12}^{\mathrm{HF}}$, contribute to $\langle b_\mathbf{k} b_{-\mathbf{k}}\rangle$. Leaving the details of the derivation to Appendix B, we present here the final answer

$$\delta S_2 = -\frac{9}{16}c_1c_2 + \frac{9}{16}(c_2 - c_1)\sum_\mathbf{k} \frac{\gamma_\mathbf{k}(1-\gamma_\mathbf{k})}{\omega_\mathbf{k}^3} + \frac{9}{4}\sum_\mathbf{k} \frac{\gamma_\mathbf{k}}{\omega_\mathbf{k}^2}\sum_\mathbf{q} \frac{\tilde{\Gamma}_1(\mathbf{q};\mathbf{k})\tilde{\Gamma}_2(\mathbf{q};-\mathbf{k})}{\omega_\mathbf{q} + \omega_{\mathbf{k}-\mathbf{q}} + \omega_\mathbf{k}} + \frac{3}{2}\sum_\mathbf{k} \frac{1 + \frac{1}{2}\gamma_\mathbf{k}}{\omega_\mathbf{k}}\sum_\mathbf{q} \frac{\tilde{\Gamma}_2(\mathbf{q};\mathbf{k})^2}{(\omega_\mathbf{q} + \omega_{\mathbf{k}+\mathbf{q}} + \omega_\mathbf{k})^2}. \tag{48}$$

This expression agrees with the formula derived previously in Ref. 11 apart from the corrected sign in front of the third term.

As is often the case with the higher-order spin-wave corrections, the individual contributions in Eq. (48) are divergent: the integrands in the second and the third terms behave as $O(1/k^3)$ at $\mathbf{k}\to\mathbf{Q}$, which means that not only the leading divergences in them, but also the subleading ones $O(1/k^2)$ must cancel in order to produce finite result. Expanding in small $\delta k = |\mathbf{k}-\mathbf{Q}|$, such a cancellation can be verified analytically.[11] Still, the expression given in Eq. (48) is not well behaved numerically. If one tries to evaluate δS_2 directly using the Monte Carlo integration, the outcome appears to be divergent. If some other methods are employed, the result may seem to be regular. We have used the simple finite sums in the $\mathbf{k}$ space that correspond to periodic clusters with the subsequent finite-size extrapolation.[16] For any given subset of (rectangular) clusters with the fixed aspect ratio the result of Eq. (48) converges to a finite value as the size of the cluster $L\to\infty$. However, as an indication of the problem, subsets with different aspect ratio yield *different* values of δS_2 in the thermodynamic limit.

The origin of the problem is the following. The internal integrals in Eq. (48) over $\mathbf{q}$ are not divergent and, generally, scale with the lattice size as[16,43]

$$\Psi_\mathbf{k}^{(L)} = \sum_\mathbf{q} {}^{(L)}F_{\mathbf{k},\mathbf{q}} = \Psi_\mathbf{k}^{(\infty)} + \frac{\alpha}{L} + \cdots. \tag{49}$$

In the thermodynamic limit, two such terms cancel near certain points and regularize the $\sim 1/k^3$ singularity in the external integral over $\mathbf{k}$,

$$\frac{1}{k^3}[\Psi_\mathbf{k}^{(\infty)} - \Phi_\mathbf{k}^{(\infty)}] = \frac{1}{k^3}[Ak^2 + \cdots]. \tag{50}$$

However, numerically such a cancellation is not complete as it carries a $1/L$ term as in Eq. (49)

$$\frac{1}{k^3}[\Psi_\mathbf{k}^{(L)} - \Phi_\mathbf{k}^{(L)}] = \frac{1}{k^3}\left[Ak^2 + \frac{\tilde{\alpha}}{L} + \cdots\right]. \tag{51}$$

Since the 2D integral of $1/k^3$ diverges as L, the $1/L$ correction from mutually canceling terms in Eq. (51) will give an unphysical contribution to the $L\to\infty$ limit of Eq. (48). This explains the erratic behavior of the numerical values of δS_2 and suggests that the extra care should be taken with Eq.

(48). The way to regularize this problem is described in Appendix B. After the regularization, the final answer for Eq. (48) can be obtained by any standard integration method, which yields

$$\delta S_2 = -0.011\,045(5). \tag{52}$$

This result differs from $\delta S_2 \approx 0.027$ quoted by Chubukov *et al.*,[11] which may have suffered from the above integration problem. Our value agrees, though, with $\delta S_2 \approx 0.011$ obtained by Miyake[10] by a different method that avoids highly singular integrals but deals with extrapolation in a small auxiliary field.

Finally,

$$\langle S \rangle = S - 0.261\,303 + \frac{0.011\,045(5)}{2S}. \tag{53}$$

Thus, the spin-1/2 Heisenberg antiferromagnet on a triangular lattice has the following value of the ordered moments—$\langle S \rangle \approx 0.249\,74$—within the second-order spin-wave expansion. Note, that this spin-wave value is somewhat larger than the results of the Green's function Monte Carlo,[14] the series-expansion,[15] and the recent DMRG calculations[16] that give $\langle S \rangle \approx 0.205(15)$.

IV. SPIN-WAVE SPECTRUM: 1/S CORRECTION

Similarly to the calculation of the static properties, perturbative expansion for the magnon spectrum has to be performed order by order in $1/S$ to ensure cancellation of all possible divergences in the individual contributions. This difficulty notwithstanding, derivation of the first $1/S$ correction to $\varepsilon_{\mathbf{k}}$ is straightforward. The anomalous terms do not contribute in that order and the new pole of the magnon Green's function is determined by

$$\varepsilon - \varepsilon_{\mathbf{k}} - \Sigma^{\mathrm{HF}}(\mathbf{k}) - \Sigma_{11}^{(a)}(\mathbf{k},\varepsilon) - \Sigma_{11}^{(b)}(\mathbf{k},\varepsilon) = 0, \tag{54}$$

to which we refer to as to the Dyson equation. The self-energies in Eq. (54) are given by the diagrams in Figs. 3(c), 4(a), and 4(b). Solving it self-consistently in the complex plane for a new renormalized spectrum $\varepsilon = \bar{\varepsilon}_{\mathbf{k}} - i\Gamma_{\mathbf{k}}$ constitutes the off-shell approximation discussed in Sec. VI.

The first-order $1/S$ correction to the spectrum is obtained within the so-called on-shell approximation. In this approximation the self-energies are evaluated at the bare magnon energy $\varepsilon = \varepsilon_{\mathbf{k}}$. This leads to the following expression for the renormalized spectrum:

$$\bar{\varepsilon}_{\mathbf{k}} - i\Gamma_{\mathbf{k}} = \varepsilon_{\mathbf{k}} + \varepsilon_{\mathbf{k}}^{(4)} - \frac{9}{4}J\sum_{\mathbf{q}}\left[\frac{\tilde{\Gamma}_1(\mathbf{q};\mathbf{k})^2}{\omega_{\mathbf{q}} + \omega_{\mathbf{k}-\mathbf{q}} - \omega_{\mathbf{k}} - i0} + \frac{\tilde{\Gamma}_2(\mathbf{q};\mathbf{k})^2}{\omega_{\mathbf{q}} + \omega_{\mathbf{k}+\mathbf{q}} + \omega_{\mathbf{k}}}\right]. \tag{55}$$

In the right-hand side the harmonic energy is $O(S)$, while the rest of the terms are $O(S^0)$. The finite magnon decay rate $\Gamma_{\mathbf{k}}$ comes only from the first term in the brackets. Since the Goldstone modes should be well defined in the ordered AFs, we expect $\Gamma_{\mathbf{k}} \ll \varepsilon_{\mathbf{k}}$ in the long-wavelength limit. The details for that limit are given in Sec. IV A, while Sec. IV B is devoted to the behavior of the renormalized spectrum in the full BZ.

A. Low-energy magnons

1. Velocity renormalization

The triangular lattice antiferromagnet has three Goldstone modes at $\mathbf{k}=0$ and $\pm\mathbf{Q}$. The existence of these zero-energy modes follows directly from the broken $SO(3)$ rotational symmetry in the spin space and, therefore, should not be affected by quantum renormalizations.[39] As a consistency check of the $1/S$ expansion, it is important to verify the presence of acoustic modes in the renormalized spectrum (55). Such a verification was first performed in Ref. 11 where the $1/S$ corrections to the velocities of the Goldstone modes were derived. We have reproduced these corrections with an improved numerical accuracy, although, technically, a somewhat different route was followed for the derivation. Numerical values of the spin-wave velocities are

$$v_0 = 3JS\frac{\sqrt{3}}{2}\left(1 - \frac{0.114\,88}{2S}\right),$$

$$v_Q = 3JS\sqrt{\frac{3}{8}}\left(1 + \frac{0.082\,85(2)}{2S}\right). \tag{56}$$

2. Long-wavelength decays

In the long-wavelength limit decay rates can be always calculated perturbatively because of the smallness of interaction among low-energy excitations and due to reduction of the phase-space volume available for decay processes. In other terms, presence of the well-defined Goldstone modes implies smallness of the damping rate with respect to their energy, $\Gamma_{\mathbf{k}} \ll \varepsilon_{\mathbf{k}}$. As with the velocity renormalization, such a behavior has to be verified using Eq. (55). As was remarked before, existence of the cubic interactions alone does not immediately yield finite lifetime for the excitations since the corresponding decays may be virtual. The decay processes become real if both the total energy and the total momentum can be conserved simultaneously. Since the two-particle excitations form a continuum of states, the energy conservation can be rephrased as the requirement of an overlap of the single-particle branch with the two-particle continuum. This yields certain kinematic conditions on the bare spectrum $\varepsilon_{\mathbf{k}}$, which are discussed in Sec. V using the example of the triangular lattice HAF. Here we assume that such conditions are fulfilled and consider several scenarios for the decays of the long-wavelength excitations relevant to the present model.

Generally, the decay rate is given by

$$\Gamma_{\mathbf{k}} \sim \sum_{\mathbf{q}} |V_{\mathbf{k},\mathbf{q}}|^2 \delta(\varepsilon_{\mathbf{k}} - \varepsilon_{\mathbf{q}} - \varepsilon_{\mathbf{k}-\mathbf{q}}), \tag{57}$$

where $V_{\mathbf{k},\mathbf{q}}$ is the decay vertex. Due to the energy conservation, the upper limit for the momentum of created quasiparticles should be of the order of k. Then, for the linear spec-

trum $\varepsilon_{\mathbf{k}} \sim k$, a naive power counting suggests the following answer:

$$\Gamma_{\mathbf{k}} \sim k^{D-1}|V_k|^2, \tag{58}$$

where k^D comes from the D-dimensional phase space, $1/k$ is due to reduction of that space to decay surface from the energy conservation, and V_k is the typical amplitude of the cubic vertex on the decay surface. Let us assume that the cubic interaction follows the standard form[29] $V_{\mathbf{k},\mathbf{q}} \propto \sqrt{kqq'}$, $q' = |\mathbf{k}-\mathbf{q}|$, and that in a typical decay process the final momenta are $q,\ q' \sim k$. This makes $|V_k|^2 \propto k^3$ and yields a seemingly universal power law for the decay rate

$$\Gamma_{\mathbf{k}} \sim k^{D+2}. \tag{59}$$

For $D=3$ this yields $\Gamma_{\mathbf{k}} \sim k^5$ which matches the result for the decays of the convex phonon branch,[44] but, as we shall see shortly, only coincidentally.

In reality, the situation is more delicate and possible power-law exponents for the decay rate asymptote depend on the specifics of the problem. In the case of a single weakly nonlinear acoustic branch, relevant to the phonon spectrum in ^{4}He,

$$\varepsilon_{\mathbf{k}} = ck + \alpha k^3, \tag{60}$$

the decays are allowed only for a positive curvature of the spectrum, $\alpha > 0$ (convex $\varepsilon_{\mathbf{k}}$). In this case, the unstable quasiparticle emits two excitations in a narrow solid angle centered in the direction of the initial momentum. The apex angle of the decay cone scales as $\theta \sim k$ such that the phase space is k^{2D-1} instead of k^D. Then the restriction from the energy conservation gives $1/k\theta^2 \sim 1/k^3$ instead of $1/k$ in the previous consideration. Altogether, for the case of the cubic upward curvature of the spectrum, the answer is universal (see also Ref. 42)

$$\Gamma_{\mathbf{k}} \sim k^{2D-1}, \tag{61}$$

which yields $\Gamma_{\mathbf{k}} \sim k^5$ in three dimensions (3D) (Refs. 29 and 44) and $\Gamma_{\mathbf{k}} \sim k^3$ in 2D. The 2D result applies to the square-lattice HAF in a strong magnetic field where the convexity of the soundlike branch changes from $\alpha < 0$ below the threshold field H^* to $\alpha > 0$ in the high-field region $H^* < H < H_s$.[36,42,37]

If several acoustic modes with different velocities are present, the fast quasiparticle can always decay into two slow ones. This situation is simpler than the previous case since the nonlinearity of the spectra plays no role. The phase-space factor becomes k^{D-1} now, in agreement with the above naive consideration. Physical realizations of this scenario include decays of the longitudinal phonon into two transverse ones in solids[28] as well as the decay of the $\mathbf{k} \to 0$ into two $\mathbf{k} \to \pm\mathbf{Q}$ magnons in the triangular lattice HAF. Clearly, such a channel of decays withstands quantum renormalization of the velocities and is pertinent to the other noncollinear AFs.

Interaction between phonons in crystals obeys the conventional scaling asymptote $V_{\mathbf{k},\mathbf{q}} \propto \sqrt{kqq'}$ and, consequently, $|V_k|^2 \propto k^3$. Therefore, the naive power counting of Eq. (59) is valid for them. However, in the case of the triangular lattice HAF, the result is yet different from Eq. (59) because the three-magnon vertex (20) is anomalous and scales as $V_{\mathbf{k},\mathbf{Q}+\mathbf{q}} \propto (q'-q)\sqrt{k/qq'}$ for small k. For a typical decay process $q,\ q' \sim k$ giving $|V_{\mathbf{k},\mathbf{Q}+\mathbf{q}}|^2 \sim k$ instead of k^3. Altogether this yields for the noncollinear HAFs in D dimensions

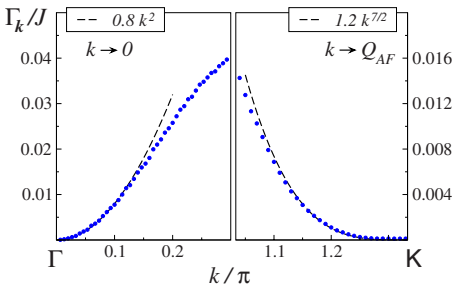

FIG. 5. (Color online) Spin-wave decay rates in the vicinity of Γ and K points in the triangular lattice HAF. Dots are numerical solutions of Eq. (55) and dashed lines are the asymptotic results (see text).

$$\Gamma_{\mathbf{k}} \sim k^D. \tag{62}$$

Direct analytic expansion of Eq. (55) gives the following decay rate of the $k \to 0$ magnons in the triangular lattice HAF ($D=2$),

$$\Gamma_{\mathbf{k}} \simeq \frac{9k^2 J}{4\sqrt{2}\pi}\left[1 + \pi\left(\frac{17}{32} - \frac{1}{2\sqrt{2}}\right)\right], \tag{63}$$

which is $\Gamma_{\mathbf{k}} \approx 0.789Jk^2$, in agreement with the numerical data in Fig. 5.

The kinematic conditions for magnons near $\pm\mathbf{Q}$ (K and K') points are more subtle. The magnon energy has a nonanalytic expansion in small $\tilde{\mathbf{k}} = \mathbf{k} - \mathbf{Q}$ with varying convexity: $\varepsilon_{\mathbf{k}} \approx c\tilde{k} + \alpha_\varphi \tilde{k}^2$, where the nonlinearity depends on the azimuthal angle $\alpha_\varphi \sim \cos 3\varphi$ [see Eq. (15)]. This form, together with the commensurability of the AF ordering vector $\mathbf{Q}$ with the reciprocal lattice of the crystal, allows for momentum and energy conservations for magnon decays from the steeper side of the energy cone at $\mathbf{k} \to \mathbf{Q}$ onto the flatter sides at $\mathbf{q},\ \mathbf{q}' \to -\mathbf{Q}$. Commensurability of $\mathbf{Q}$ is important here as $3\mathbf{Q} = 0$ is the necessary condition for the conservation of the quasimomentum. Thus, magnons near the $\mathbf{Q}$ point are unstable only in a certain range of angles. The decay vertex for $\mathbf{k} \to \mathbf{Q}$ magnon has the conventional scaling $V_{\mathbf{Q}+\mathbf{k},-\mathbf{Q}+\mathbf{q}} \propto \sqrt{kqq'}$, so the decay probability is $|V_k|^2 \sim k^3$. However, due to a constraint on the angle between $\mathbf{k}$ and $\mathbf{q}$, the decay surface in $\mathbf{q}$ space is a cigar-shaped ellipse with length $\sim k$ and width $\sim k^{3/2}$. That makes the restricted phase volume of decays to scale as $k^{(3D-5)/2}$. This results in a nontrivial law

$$\Gamma_{\mathbf{k}} \sim k^{(3D+1)/2}, \tag{64}$$

which gives $k^{7/2}$ for the decay rate in 2D. Numerically, along the $K\Gamma$ line $\Gamma_{\mathbf{k}} \approx 1.2Jk^{7/2}$ (see Fig. 5). Away from this direction the damping exhibits an anomalous angular dependence $\Gamma_{\mathbf{k}} \sim 1/(\cos 3\varphi)^{3/2}$. Such a behavior is related to the saddle-point singularities which is discussed in Sec. V.

B. High-energy magnons

The renormalized spin-wave energy and the magnon damping given by Eq. (55) have been calculated using the

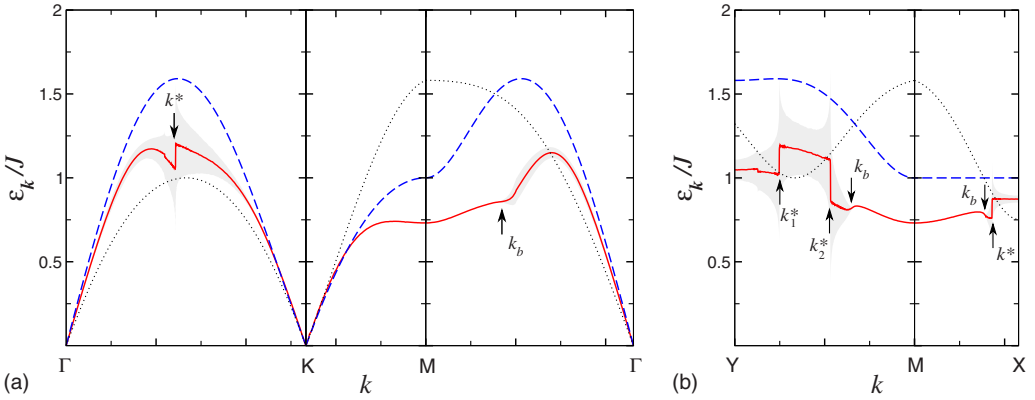

FIG. 6. (Color online) Spin-wave energy for the $S=1/2$ triangular lattice HAF along the symmetry directions in the BZ. Dashed and solid lines are the results obtained in the LSWT approximation ($\varepsilon_{\mathbf{k}}$) and with the first-order $1/S$ correction ($\bar{\varepsilon}_{\mathbf{k}}$), respectively. Vertical arrows indicate singularities and intersection points with the two-magnon continuum. Gray areas show the width of the spectral peaks due to damping $\Gamma_{\mathbf{k}}$ from Fig. 7. Dotted lines represent the minimum of the two-magnon continuum obtained from the LSWT spectrum.

Monte Carlo integration method with 10^8-10^9 integration points in the full BZ. Numerical results for the spin-1/2 case are shown in Figs. 6 and 7 for representative symmetry directions in the BZ (see Fig. 2 for notations). Statistical errors of the calculation are comparable or smaller than the corresponding linewidth. The first prominent feature of the spectrum is that the renormalization is stronger at large momenta, in a qualitative agreement with the series-expansion results.[15,19,20] As we have argued before, this is a consequence of the considerable coupling between single-magnon excitations and two-magnon continuum determined by cubic anharmonicities. The momentum dependence of the minimum of the continuum is shown in Fig. 6 by dotted curves. The intersection points of these curves with the magnon branch are marked as k_b's. Inside the continuum, magnon excitations become intrinsically damped acquiring a nonzero $\Gamma_{\mathbf{k}}$ (see Fig. 7). The magnitude of the overlap of the continuum with the single-particle branch gives a qualitative idea of the phase space available for decays. The damping rate is also illustrated in Fig. 6 as the shaded area between $\bar{\varepsilon}_{\mathbf{k}}-\Gamma_{\mathbf{k}}$ and $\bar{\varepsilon}_{\mathbf{k}}+\Gamma_{\mathbf{k}}$.

Another interesting property of the renormalized spectrum in Fig. 6 is its shape in the vicinity of the M point (edge center of the BZ). Quantum renormalization converts the saddle point of $\varepsilon_{\mathbf{k}}$ at $\mathbf{k}_M$ into a local minimum surrounded by flat parts.[15,18,19] Such local extrema must contribute significantly to the thermodynamic properties of the triangular lattice HAF.[15,18] The minimum in $\bar{\varepsilon}_{\mathbf{k}}$ is more pronounced in the numerical results[15] than in Fig. 6. It was called a rotonlike minimum and it was suggested that it might be a signature of spinons.[18] This has been questioned later since the same feature in the spin-wave results can be explained by the enhanced density of two-magnon states near the M point.[19,20]

Although the above discussion is important for benchmarking the spin-wave theory with the series-expansion results, the most remarkable property of the renormalized spectrum is the substantial jumplike discontinuities in $\bar{\varepsilon}_{\mathbf{k}}$, marked as k^* points in Fig. 6, with the jump heights reaching 1/4 of the magnon bandwidth. If considered without the concomitant behavior of $\Gamma_{\mathbf{k}}$, such jumps in $\bar{\varepsilon}_{\mathbf{k}}$ are especially enigmatic. The values of the damping at the top of the magnon band are also quite substantial, leading to broadening of the spectral peaks with the widths about $(2\Gamma_{\mathbf{k}}/\bar{\varepsilon}_{\mathbf{k}})\sim 1/3$. The most striking features of $\Gamma_{\mathbf{k}}$ are the sharp logarithmic singularities at several points along the selected cuts of the Brillouin zone. These are precisely the same k^* points where the jumps occur in the real part of the spectrum. Thus, the two singularities are intrinsically related. Analytic consideration

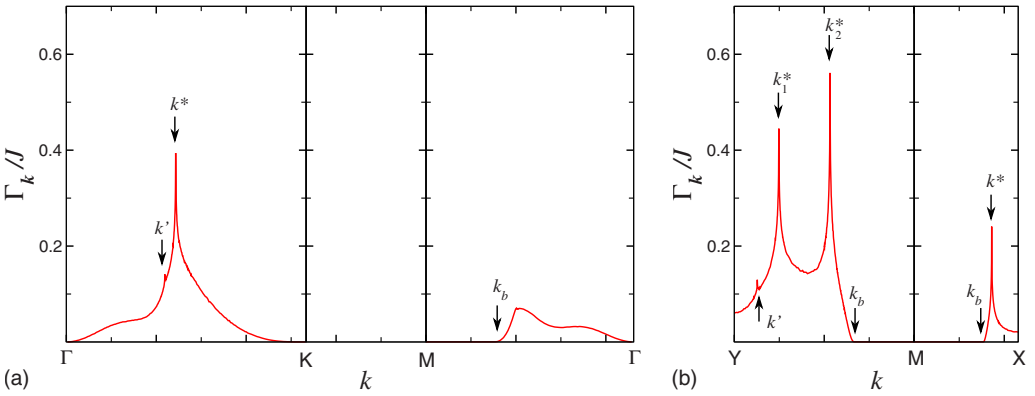

FIG. 7. (Color online) The spin-wave damping of the $S=1/2$ triangular lattice HAF calculated in the first order of the $1/S$ expansion along the same lines as in Fig. 6. Arrows indicate singularities and intersection points with the two-magnon continuum.

of these singularities in the magnon self-energy is presented in Sec. V B. Here we simply state that their origin is due to the intersection of the single-magnon branch with the line of the van Hove saddle-point singularities in the two-magnon continuum.

The logarithmic singularities in the damping rate signify a breakdown of the $1/S$ expansion in the vicinity of the singular k^* points. It is remarkable that the log singularities are obtained already in the lowest-order interacting spin-wave theory. Therefore, if any other property calculated with the $1/S$ expansion is to be compared to numerical methods, such singularities must be understood and their proper treatment within the theory outlined. Note, that the numerical series-expansion results exhibit lack of convergence (large error bars) at certain $\mathbf{k}$ points.[18] Although, this is not the same as singular jumps, such numerical features might occur due to similar reasons. Analytic results for the spectrum near the singularities and the proper treatment of the latter will be presented in Secs. V and VI, respectively.

Altogether, the main effects of quantum fluctuations in the spectrum of the triangular lattice HAF are the substantial magnon damping in the major part of the BZ, singular behavior of the decay rate along certain contours in the $\mathbf{k}$ space, and strong downward renormalization of the magnon energies compared to the harmonic spin-wave theory. All these effects underline the importance of cubic anharmonicities in the noncollinear AFs and represent major qualitative differences from the collinear cases.

V. KINEMATICS OF TWO-PARTICLE DECAYS

The aim of this section is to consider kinematic constraints that follow from the energy conservation in the two-particle decay process

$$\varepsilon_{\mathbf{k}} = \varepsilon_{\mathbf{q}} + \varepsilon_{\mathbf{k}-\mathbf{q}}. \tag{65}$$

This equation should be treated as an equation in $\mathbf{q}$ with the initial momentum $\mathbf{k}$ as a parameter. The solutions of Eq. (65) form the *decay surface* in the $\mathbf{q}$ space. Examples of the decay surfaces (contours in 2D) for the triangular lattice HAF are shown in Fig. 8 for a few representative $\mathbf{k}$ points along the ΓK line.

As a function of $\mathbf{k}$, the decay surface changes and may disappear completely. In such a case, particles become stable with $\Gamma_{\mathbf{k}} \equiv 0$. The region in the $\mathbf{k}$ space with stable excitations is separated from the decay region by the *decay threshold boundary*. Generally, two-particle excitations form a continuum of states in a certain energy interval

$$E_{\mathbf{k}}^{\min} \leq E_{\mathbf{k}}(\mathbf{q}) \equiv \varepsilon_{\mathbf{q}} + \varepsilon_{\mathbf{k}-\mathbf{q}} \leq E_{\mathbf{k}}^{\max}. \tag{66}$$

Thus, the decay threshold boundary is determined by the intersection of the single-particle branch $\varepsilon_{\mathbf{k}}$ with the bottom of the continuum $E_{\mathbf{k}}^{\min}$. For our problem, the decay region is the hexagram shown in Fig. 9.

Needless to say, the two-particle decays may be prohibited in the entire BZ, a situation that is common for collinear antiferromagnets in zero field.[27] In such a case, spontaneous n-particle decays with $n>2$ are also prohibited since all the energies in the n-particle generalization of Eq. (65) are positively defined. Thus, the analysis of the two-particle decay conditions is crucial for determining whether any spontaneous decays are possible. In the case when the two-particle decay region is finite, the n-particle decays can, in principle, be allowed in a wider region of the $\mathbf{k}$ space (see, e.g., the corresponding study for the phonon branch in ^{4}He).[45] However, such an expansion of the decay region requires rather special conditions and is not discussed in this work.

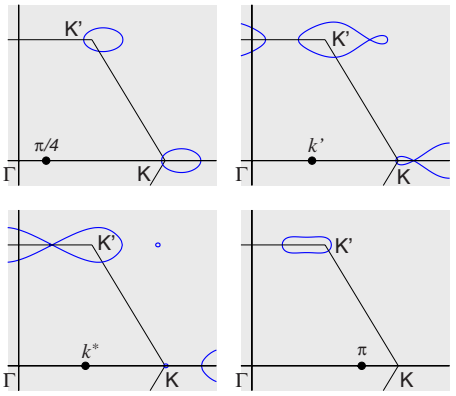

FIG. 8. (Color online) The decay contours in $\mathbf{q}$ space for magnons with selected $\mathbf{k}$'s along the ΓK direction; $k=k'$ and $k=k^*$ are the same as in Fig. 7, left panel. The corresponding $\mathbf{q}$ contours undergo topological transitions at k' and k^*.

Aside from finding whether spontaneous decays exist or not, there is another important reason for considering the decay kinematics. As was emphasized by Pitaevskii[29,46] in the analysis of the two-roton decay threshold in superfluid ^{4}He, the enhanced density of two-particle states near the minimum of the continuum may produce strong singularities in the single-particle spectrum at the decay boundary. This yields various unusual effects,[29,30,46] including complete disappearance of the quasiparticle branch inside the continuum. Apart from the singularities in the spectrum at the decay boundary, additional singularities may occur within the decay region due to topological transitions of the decay surface.[20] General analysis of these two effects and its application to the triangular HAF are discussed here.

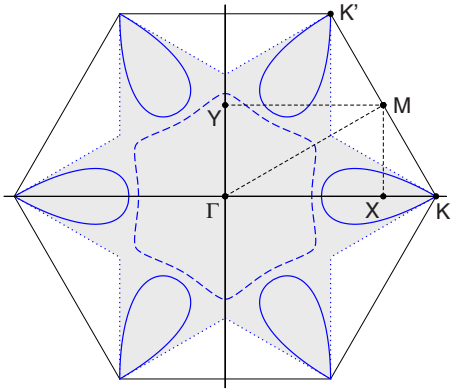

FIG. 9. (Color online) The Brillouin zone of a triangular lattice. Shaded area shows the region where spontaneous two-magnon decays are allowed. Lines correspond to the extrema in the two-magnon continuum described in text.

A. Decay threshold boundary

The boundary of the decay region corresponds to the intersection of the single-particle branch $\varepsilon_{\mathbf{k}}$ with the bottom of the two-particle continuum (66). To find $E_{\mathbf{k}}^{\min}$ one should analyze the extrema of the continuum given by

$$\frac{\partial E_{\mathbf{k}}(\mathbf{q})}{\partial \mathbf{q}} = \left.\frac{\partial \varepsilon_{\mathbf{q}}}{\partial \mathbf{q}}\right|_{\mathbf{q}} - \left.\frac{\partial \varepsilon_{\mathbf{q}}}{\partial \mathbf{q}}\right|_{\mathbf{k}-\mathbf{q}} = 0. \tag{67}$$

Thus, the extremum condition is satisfied if the *velocities* of the decay products are equal. This yields D equations with $\mathbf{q}$ and $\mathbf{k}$ as independent variables. To find the decay boundary one needs to solve the decay and the extremum conditions (65) and (67) together. Solving them yields a set of $(D-1)$-dimensional surfaces in the $\mathbf{k}$ space. Since the nontrivial solution may exist not only for the minimum of the continuum but for the other extrema as well, some parts of these surfaces define the decay threshold boundary while the rest of the solutions will correspond to the special surfaces within the decay region. The latter is considered in Sec. V B.

For the gapless spectrum, one should also verify whether the emission of the acoustic (Goldstone) excitation at $\mathbf{q} \rightarrow \mathbf{Q}_i$ corresponds to $E_{\mathbf{k}}^{\min}$. This condition is separate from Eq. (67) as the Goldstone modes are not the extrema but the end points of the spectrum. In the case when one or more of these gapless modes define $E_{\mathbf{k}}^{\min}$, the decay boundary is given by

$$\varepsilon_{\mathbf{k}} = \varepsilon_{\mathbf{k}+\mathbf{Q}_i}. \tag{68}$$

Although the above discussion covers two most general cases, there exists a particular form of the solution of Eqs. (65) and (67) for which finding the threshold boundary simplifies greatly. The two-particle continuum always possesses an extremum when both decay products have equal momenta, up to a reciprocal-lattice vector $\mathbf{G}$: $\mathbf{q},\mathbf{k}-\mathbf{q} = (\mathbf{k}+\mathbf{G})/2$. The condition of equal velocities (67) is automatically satisfied in this case. Such an extremum crosses with the single-particle branch on the surface determined by

$$\varepsilon_{\mathbf{k}} = 2\varepsilon_{(\mathbf{k}+\mathbf{G})/2}. \tag{69}$$

Among the previously studied cases, the decay boundaries for the square- and cubic-lattice HAFs in a strong external field satisfy the above equation.[36]

For the case of the triangular lattice HAF, let us begin with the analysis of the decay involving the Goldstone modes. The acoustic branch emerging from $\mathbf{q}=0$ does not correspond to the crossing point of $\varepsilon_{\mathbf{k}}$ and $E_{\mathbf{k}}^{\min}$ and should be disregarded. The condition (68) on the emission of Goldstone modes with $\mathbf{q}=\pm\mathbf{Q}$ can be rewritten, using the expression (12) for the harmonic spectrum, as $\gamma_{\mathbf{k}}=\gamma_{\mathbf{k}\mp\mathbf{Q}}$. This last equation is easily solved and the results are shown in Fig. 9 by the dotted lines. One can show that $\mathbf{q}=\pm\mathbf{Q}$ points correspond to the absolute minimum of the continuum for all $\mathbf{k}$ within the shaded area in Fig. 9. To demonstrate that, $\varepsilon_{\mathbf{k}\pm\mathbf{Q}}$ is also plotted in Fig. 6 as dotted line.

We begin the analysis of the extrema in the two-particle continuum with the decay threshold involving magnons with equal momenta. The solutions of Eq. (69) for the reciprocal-lattice vectors $\mathbf{G}_{1,2}=(\pm 2\pi, 2\pi/\sqrt{3})$ and $\mathbf{G}_3=(0,4\pi/\sqrt{3})$ are readily found numerically and are shown in Fig. 9 by solid lines. No solution exists for $\mathbf{G}=0$. Solid lines in Fig. 9 lie entirely within the shaded area and correspond to the saddle points of the continuum, not the minima. The solution for the general situation of the threshold decay into a pair of nonidentical magnons with equal velocities but different momenta and energies, $\varepsilon_{\mathbf{k}-\mathbf{q}} \neq \varepsilon_{\mathbf{q}}$, is obtained by solving numerically the decay (65) and extremum (67) conditions simultaneously. The result is plotted in Fig. 9 by the dashed line. As in the previous case, this contour corresponds to the line of saddle points of the continuum within the decay region.

Altogether, the decay region is given by the union of all areas obtained in the above three cases. As one can see, the decay threshold boundary in the triangular HAF is determined entirely by the emission of acoustic $\varepsilon_{\pm\mathbf{Q}}$ magnon. In accordance with the long-wavelength consideration of Sec. IV A, the area around $\mathbf{k}=0$ is precisely where the decay of the fast magnon $\varepsilon_{\mathbf{k}\rightarrow 0}$ into two slow ones $\varepsilon_{\mathbf{q}\rightarrow\pm\mathbf{Q}}$ takes place and this area is completely enclosed in the decay region. Similarly, there are only finite segments in the vicinity of the $\pm\mathbf{Q}$ points where decays are possible. The other thresholds due to two-magnon extrema do not contribute to the decay boundary. As is shown in Sec. VII, such a mutual arrangement of different thresholds may or may not be the case for other closely related systems. Already a simple addition of the XXZ anisotropy modifies the decay boundary and switches saddle points into minima for certain momenta.

The damping of magnons close to the boundary of the decay region can be considered in a manner similar to the long-wavelength analysis of Sec. IV A 2. Since the velocity of the decaying magnon near the boundary must be larger than the velocity of the emitted acoustic $\pm\mathbf{Q}$ mode, the phase-space factor is $(k-k_b)^{D-1}$ as is given in Eq. (58). The probability of the decay has a smallness only with respect to $q \sim (k-k_b)$. This yields the 2D decay rate near the threshold due to acoustic mode

$$\Gamma_{\mathbf{k}} \sim (k-k_b)^2, \tag{70}$$

in agreement with the results in Fig. 7 in the vicinity of k_b points.

B. Topological transition in the decay surface

A truly remarkable feature of the magnon spectrum in the triangular lattice HAF is the logarithmic peaks in $\Gamma_{\mathbf{k}}$ obtained in the first order of $1/S$ expansion. After preceding discussion it is clear that the location of such singularities corresponds to the crossing of single-magnon branch with the surface of saddle points of two-magnon continuum. Indeed, the k^* points in Figs. 6 and 7 belong to the threshold contour for the decays into pairs of equivalent magnons (solid lines in Fig. 9). Much weaker anomalies, which are visible only as small peaks in $\Gamma_{\mathbf{k}}$ that are denoted by k''s in Fig. 7, correspond to the threshold contour for the decays into nonequivalent magnons (dashed lines in Fig. 9).

In the vicinity of the crossing points of the single-particle branch with the saddle-point surface of the continuum, the magnon *decay surface* undergoes a topological transition

(see Fig. 8). Expanding the energy conservation condition (65) in small $\Delta\mathbf{k}=\mathbf{k}-\mathbf{k}^*$ and $\Delta\mathbf{q}=\mathbf{q}-\mathbf{q}^*$, where $\mathbf{k}^*$ is the point on the threshold contour and $\mathbf{q}^*$ is the saddle point of $E_{\mathbf{k}^*}(\mathbf{q})$, we obtain

$$\varepsilon_{\mathbf{k}}-\varepsilon_{\mathbf{q}}-\varepsilon_{\mathbf{k}-\mathbf{q}}\approx(\mathbf{v}_1-\mathbf{v}_2)\cdot\Delta\mathbf{k}-\frac{\Delta q_x^2}{a^2}+\frac{\Delta q_y^2}{b^2}=0, \quad (71)$$

where $\mathbf{v}_1$ and $\mathbf{v}_2$ are the velocities of the initial and final magnons and a, b are constants. Depending on the sign of $(v_1-v_2)\Delta k$ the solutions of the above equation are two conjugate hyperbolas, which transform into a pair of crossing lines for $\Delta\mathbf{k}=0$. Thus, $\mathbf{k}=\mathbf{k}^*$ corresponds to the point where the decay surface splits into two disjoint pieces, as is indeed observed in Fig. 8.

The discussions in terms of saddle points of the continuum and topological transitions of the decay surface complement each other. While the van Hove singularities are always present in the two-magnon continuum (66) they do not necessarily cross with the one-magnon branch. On the other hand, using the topological transition perspective one can argue that the occurrence of such a crossing does not depend on a precise form of $\varepsilon_{\mathbf{k}}$. As was discussed in Sec. IV A, acoustic magnon with small $\mathbf{k}$ decays into two magnons that are close to $\mathbf{Q}$ and $-\mathbf{Q}$. Its decay surface consists of two disjoint parts near K and K' points (see $k_x=\pi/4$ in Fig. 8). Similarly, a magnon with $\mathbf{k}\to\mathbf{Q}$ can emit two magnons in the vicinity of $-\mathbf{Q}$. The corresponding decay surface is a single closed contour near the K' point (see $k_x=\pi$ in Fig. 8). Therefore, moving along an arbitrary trajectory in $\mathbf{k}$ space between Γ and K points the decay surface must undergo at least one topological transformation, which also implies crossing of at least one saddle-point threshold contour. The actual number of such transformations is determined by the short-wavelength details of the spectrum. For the triangular lattice HAF there are two of them as is demonstrated in Figs. 8 and 9.

Let us now consider behavior of the magnon self-energy in the vicinity of singular points. The decay vertex is regular at $\mathbf{k}\to\mathbf{k}^*$ and $\mathbf{q}\to\mathbf{q}^*$ and gives an unimportant constant factor. Using the expansion (71) we obtain for the singular part of the magnon self-energy

$$\Sigma(\mathbf{k},\varepsilon_{\mathbf{k}})\propto\int\frac{d^2q}{(v_1-v_2)\Delta k-q_x^2/a^2+q_y^2/b^2+i0}. \quad (72)$$

A straightforward integration in Eq. (72) yields

$$\mathrm{Re}\,\Sigma(\mathbf{k},\varepsilon_{\mathbf{k}})\simeq\mathrm{sgn}(\Delta k), \quad \Gamma_{\mathbf{k}}\simeq\ln\frac{\Lambda}{|\Delta k|}, \quad (73)$$

where $\Gamma_{\mathbf{k}}\equiv-\mathrm{Im}\,\Sigma(\mathbf{k},\varepsilon_{\mathbf{k}})$. The cut-off parameter Λ is determined by the characteristic size of the region in the $\mathbf{k}$ space where the expansion (71) holds. The linear size of the smallest "droplet" of the decay surface at the topological transition can be taken as an upper bound on Λ (see Fig. 8). Such an estimate explains the difference in the strength of anomalies in $\Gamma_{\mathbf{k}}$ for k^* and k' points. The topological transition at k^* consists of joining/splitting of the two approximately equal contours of substantial size, while the k' point corresponds to the splitting off of a small piece.

To put this discussion in a broader context we note than in the earlier works[29,36,46] the situation was considered when a singularity occurs at the boundary of the decay region rather than in the interior. In such a case, the extremum in the two-particle continuum that is crossed by the single-particle branch is a minimum, not a saddle-point, and the analog of Eq. (72) for $\Sigma(\mathbf{k},\varepsilon_{\mathbf{k}})$ is given by

$$\Sigma(\mathbf{k},\varepsilon_{\mathbf{k}})\propto\int\frac{d^2q}{(v_1-v_2)\Delta k-q_x^2/a^2-q_y^2/b^2+i0}. \quad (74)$$

After integration this yields the following characteristic anomaly:

$$\mathrm{Re}\,\Sigma(\mathbf{k},\varepsilon_{\mathbf{k}})\simeq\ln\frac{\Lambda}{|\Delta k|}, \quad \Gamma_{\mathbf{k}}\simeq\Theta(\Delta k), \quad (75)$$

where $\Theta(x)$ is the Heaviside step function. Thus, the situation is reversed in comparison to our case: the log anomaly occurs in the real part and the jump in the imaginary part of the spectrum. Since the imaginary part of $\Sigma(\mathbf{k},\varepsilon_{\mathbf{k}})$ is related to the two-particle density of states, in 2D it is natural to have a jump in $\Gamma_{\mathbf{k}}$ upon entering the continuum and a log singularity upon crossing the saddle-point line inside the continuum. By the Kramers-Kronig relations such jumps and logs in $\mathrm{Im}\,\Sigma(\mathbf{k},\varepsilon_{\mathbf{k}})$ result in logs and jumps in $\mathrm{Re}\,\Sigma(\mathbf{k},\varepsilon_{\mathbf{k}})$, respectively. For the 3D systems, logarithmic peaks disappear and one obtains only square-root singularity $\mathrm{Re}\,\Sigma(\mathbf{k},\varepsilon_{\mathbf{k}})\simeq\sqrt{|\Delta k|}$.

Another important question concerns whether singularities in the spectrum will survive the higher-order $1/S$ treatment. If the singularity persists, vertex corrections may become important (see Appendix C).[29] Our Sec. VI discusses this problem.

VI. OFF-SHELL DYSON EQUATION AND SPECTRAL FUNCTION

The unusual logarithmic singularities in the magnon decay rate $\Gamma_{\mathbf{k}}$ found in the first-order $1/S$ corrections signify a breakdown of the standard spin-wave expansion. They represent an extra theoretical challenge and have to be renormalized in order to obtain the actual dynamical behavior. The purpose of this section is to describe, at a technical level, different approaches to this problem. In Sec. VI A we show that the singularities are regularized, for the most part, by allowing for the finite lifetime of the magnon in the *initial* state within the so-called off-shell approach. However, in the strong-coupling case, the single-particle excitation may disappear in the vicinity of the singularity, similar to the termination point in the quasiparticle spectrum of superfluid ^{4}He.[46] In Sec. VI B we discuss the magnon spectral function $A(\mathbf{k},\omega)$ and find additional singularities in the ω space that are directly connected to the van Hove singularities in the two-magnon continuum.

A. Singularities and off-shell solution

1. Modified decay region

The first-order quantum correction to the magnon dispersion (Sec. IV) leads to a significant narrowing of the magnon

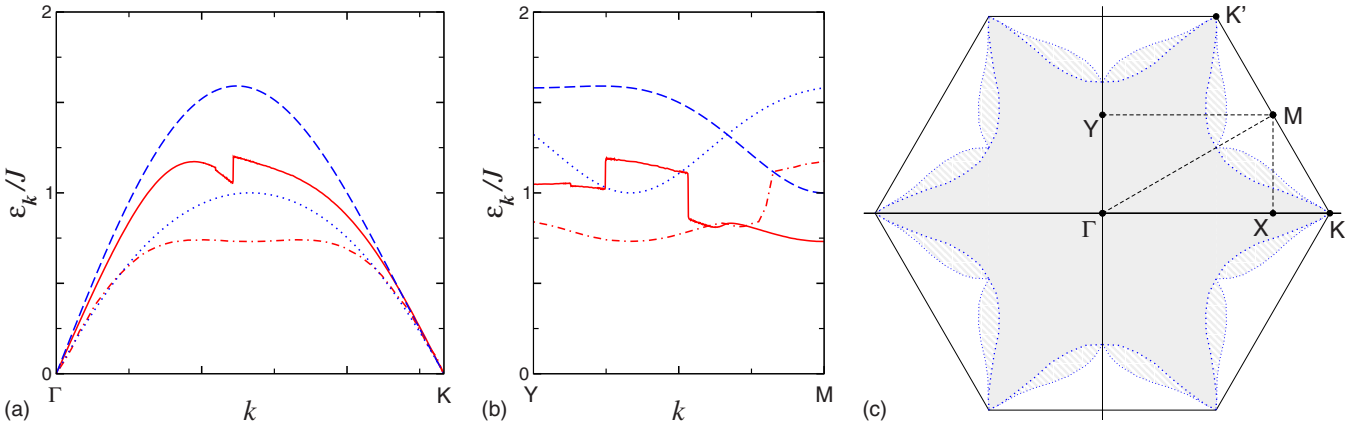

FIG. 10. (Color online) Renormalization of the decay region for the spin-1/2 triangular lattice HAF. Left and middle panels: Dashed and dotted lines are the LSWT predictions for the magnon dispersion $\varepsilon_{\mathbf{k}}$ (dashed) and for the minimum of the two-magnon continuum (dotted); solid and dotted-dashed lines represent same results for the spectrum $\bar{\varepsilon}_{\mathbf{k}}$ with the first-order quantum correction, respectively. Right panel: Modified decay region; lightly shaded regions highlight the area of uncertainty due to the re-entrant behavior seen in the middle panel.

bandwidth for the spin-1/2 triangular lattice HAF. Therefore, one may ask how strongly the spectrum renormalization affects the decay boundary and whether the decay condition Eq. (65) is still satisfied for the *renormalized* $\bar{\varepsilon}_{\mathbf{k}}$. In the long-wavelength limit, the difference between the velocities of the acoustic modes $v_0 > v_Q$ [see Eq. (56)] guarantees that the kinematic conditions for decays at $\mathbf{k} \to 0$ are always fulfilled. While this argument is applicable to any system with several types of the Goldstone mode, the decay boundary is defined by the short-wavelength features, specific to a particular system.

In Fig. 10 we present numerical results, which show that the size of the decay region does not change appreciably even for the $S=1/2$ triangular lattice HAF. The left and the middle panels demonstrate the renormalization of the bottom of the two-magnon continuum for two representative paths in the BZ. The lowest-energy two-magnon states within the decay region still correspond to the emission of the $\pm\mathbf{Q}$ Goldstone mode, $\bar{E}^{\min}_{\mathbf{k}} = \bar{\varepsilon}_{\mathbf{k}\pm\mathbf{Q}}$. While the renormalizations of the spectrum and the continuum are significant, the intersection points of the two change only weakly. For the YM path in the BZ (see Fig. 9) one observes a re-entrant crossing of the single-magnon branch with the bottom of the continuum, which leaves some uncertainty in defining the new decay boundary. This behavior is related to the jumplike singularities in the single magnon $\bar{\varepsilon}_{\mathbf{k}}$, which should become more well behaved once the singularities are regularized. The right panel of Fig. 10 presents the "new" magnon decay boundary for the spectrum that includes $1/S$ renormalization. The light-shaded regions show the uncertainty areas where the re-entrant behavior of the spectrum and the continuum occur. Overall, the decay region does not change significantly in comparison to the LSWT boundary in Fig. 9.

2. Higher-order diagrams perspective

One way to regularize the decay diagram is to allow for a finite lifetime of the decay products by dressing the inner lines in the "bubbles" in Fig. 4. The effect of such a dressing depends, however, on whether the saddle-point momenta of the decay products $\mathbf{q}^*$ and $\mathbf{k}^* - \mathbf{q}^*$ in Fig. 8 fall inside or outside of the decay region. If $\mathbf{q}^*$ lies inside the decay region for at least one of the final magnons, then this magnon will acquire a finite lifetime in the next order. The logarithmic singularity in $\Gamma_{\mathbf{k}}$ will be removed in this case since the energy conservation law Eq. (65) is now satisfied only on average. For the triangular lattice HAF such a scenario is realized for a large fraction of the "weak" singularities (k' points in Figs. 6 and 7). However, all of the "strong" singularities (k^* points in Figs. 6 and 7) and some of the "weak" ones belong to another class in which the saddle points for both magnons created in the decay process are *outside* of the decay region. Hence, at the saddle points, the logarithmic divergence of the one-loop diagrams will persist even for the renormalized spectrum and the singularities seems to remain essential.

Thus, the above approach requires summation of an infinite series of diagrams that contain leading-order divergences, similar to the Pitaevskii's treatment of the spectrum termination problem.[29,46] Such a treatment is hindered within the spin-wave theory by the divergence of the individual terms at $\mathbf{k} \to \mathbf{Q}$ in each order of the $1/S$ expansion, the problem already mentioned in Secs. III and IV. While a qualitative statement on the result of such a regularization can be made (see Appendix C) any quantitatively reliable calculation is problematic in the light of this problem.

3. Off-shell Dyson equation

The above seemingly hopeless situation is resolved if we note that the logarithmic singularity occurs for a magnon which is inside the decay region. This means that the Dyson Eq. (54) should be solved "off shell," i.e., with the same complex energy $\varepsilon = \bar{\varepsilon}_{\mathbf{k}} - i\Gamma_{\mathbf{k}}$ both outside and inside $\Sigma(\mathbf{k}, \varepsilon)$. Physically, such a procedure allows for a finite lifetime of the *initial* magnon while magnons created during the decay process remain stable. The off-shell approach avoids complications related to multiloop diagrams and, as we demonstrate below, is sufficient to regularize the singularity. Note that the magnon energy in the off-shell solution contains corrections

beyond the first $1/S$ order. Nevertheless, it can be shown that it is yet free from the $\mathbf{k}\to\mathbf{Q}$ divergences associated with the higher-order diagrams mentioned above.

After a methodological remark made in Appendix D on the proper sign of the imaginary part of ε in the decaylike self-energy, the Dyson Eq. (54) is given by

$$\varepsilon - \varepsilon_{\mathbf{k}} - \Sigma(\mathbf{k},\varepsilon^*) = 0, \tag{76}$$

where ε^* is the complex conjugate of ε and $\Sigma(\mathbf{k},\varepsilon)$ includes all one-loop contributions given by Eq. (54). Rewriting the above equation explicitly for the real and imaginary parts one obtains the following system:

$$\bar{\varepsilon}_{\mathbf{k}} = \varepsilon_{\mathbf{k}} + \mathrm{Re}[\Sigma(\mathbf{k},\bar{\varepsilon}_{\mathbf{k}} + i\Gamma_{\mathbf{k}})],$$

$$\Gamma_{\mathbf{k}} = -\mathrm{Im}[\Sigma(\mathbf{k},\bar{\varepsilon}_{\mathbf{k}} + i\Gamma_{\mathbf{k}})] > 0. \tag{77}$$

Let us first demonstrate how a finite $\Gamma_{\mathbf{k}}$ can regularize the singularity. Replacing $\varepsilon_{\mathbf{k}}$ in Eq. (71) with complex ε and using parametrization $\varepsilon-\varepsilon_c-\mathbf{v}_2\cdot\Delta\mathbf{k}=\bar{\rho}=|\bar{\rho}|e^{-i\varphi}$, where ε_c is the position of the saddle point in the continuum, we obtain after integration

$$\Sigma(\mathbf{k},\varepsilon) \simeq -\frac{V_3^2}{JS}\left[\left(\frac{\pi}{2}-\varphi\right) + i\,\ln\left|\frac{\Lambda JS}{\bar{\rho}}\right|\right]. \tag{78}$$

Here, $V_3^2\propto\Gamma_1^2(\mathbf{k}^*,\mathbf{q}^*)\sim J^2S$ and Λ is the momentum cutoff. Omitting the nonsingular contributions, Eq. (77) is rewritten as

$$\bar{\varepsilon}_{\mathbf{k}} \simeq \varepsilon_{\mathbf{k}} - \frac{V_3^2}{JS}\left(\frac{\pi}{2}-\varphi\right),$$

$$\Gamma_{\mathbf{k}} \simeq \frac{V_3^2}{JS}\ln\left|\frac{\Lambda JS}{\bar{\varepsilon}_{\mathbf{k}} - \varepsilon_c - \mathbf{v}_2\cdot\Delta\mathbf{k} + i\Gamma_{\mathbf{k}}}\right|. \tag{79}$$

The on-shell solution is recovered by substituting $\varepsilon_{\mathbf{k}}=\varepsilon_c+\mathbf{v}_1\cdot\Delta\mathbf{k}$ instead of $\varepsilon=\bar{\varepsilon}_{\mathbf{k}}+i\Gamma_{\mathbf{k}}$ in Eq. (79). This yields $\bar{\rho}=(\mathbf{v}_1-\mathbf{v}_2)\cdot\Delta\mathbf{k}$ and also implies that $\cos\varphi=\pm1$ (or $\varphi=0,\pi$) depending on the sign of Δk. As a result, one finds the jump in the real part of the spectrum and the log singularity in the decay rate in agreement with Eq. (73).

Any renormalization should shift the "bare" singularity into a new crossing point of the single-magnon branch with the surface of the saddle points in the two-magnon continuum. Assuming that the real part of the energy renormalization is already included in the definition of ε_c and $\mathbf{k}^*$ and that $\bar{\varepsilon}_{\mathbf{k}}$ can be still expanded as $\bar{\varepsilon}_{\mathbf{k}}\simeq\varepsilon_c+\mathbf{v}_1\cdot\Delta\mathbf{k}$ we obtain

$$\Gamma_{\mathbf{k}} \simeq \frac{V_3^2}{JS}\ln\left|\frac{\Lambda JS}{\Delta\mathbf{v}\cdot\Delta\mathbf{k} + i\Gamma_{\mathbf{k}}}\right|. \tag{80}$$

As a result, the imaginary part of the solution at the singular point $\Delta\mathbf{k}$ is now regular and can be determined by solving the transcendental equation

$$\gamma^* = \ln\left(\frac{\Lambda(JS)^2}{V_3^2}\frac{1}{\gamma^*}\right), \tag{81}$$

with $\Gamma_{\mathbf{k}}=V_3^2\gamma^*/JS$. Depending on the relative strength of the three-magnon coupling $(V_3/JS)^2$ to the size of the dimensionless momentum cutoff Λ there are two different regimes,

$$\Gamma_{\mathbf{k}} \simeq \frac{V_3^2}{JS}\ln\left[\frac{\Lambda(JS)^2}{V_3^2}\right], \quad V_3^2/\Lambda(JS)^2 \ll 1,$$

$$\Gamma_{\mathbf{k}} \simeq \Lambda JS, \quad V_3^2/\Lambda(JS)^2 \gg 1. \tag{82}$$

Thus, at large $V_3^2/\Lambda(JS)^2$ the decay rate is independent of the coupling and is defined by the phase volume factor. Recalling that $V_3^2\propto J^2S$ in the case of the triangular lattice HAF, we obtain estimates

$$\frac{\Gamma_{\mathbf{k}}}{JS} \propto \frac{1}{S}\ln(S\Lambda), \quad S\Lambda \gg 1,$$

$$\frac{\Gamma_{\mathbf{k}}}{JS} \propto \Lambda, \quad S\Lambda \ll 1, \tag{83}$$

where the first expression is relevant to the "strong" singularities with large phase-space volume for decays (k^* points) and the second is for the "weak" ones (k' points).

For $\mathbf{k}\to\mathbf{k}^*$, one finds for the off-shell solution

$$\cos\varphi = \frac{\mathrm{Re}(\Delta\varepsilon - \mathbf{v}_2\cdot\Delta\mathbf{k})}{|\Delta\varepsilon - \mathbf{v}_2\cdot\Delta\mathbf{k}|} \approx \frac{\Delta\mathbf{v}\cdot\Delta\mathbf{k}}{\Gamma_{\mathbf{k}}} \to 0. \tag{84}$$

Hence, $\varphi\to\pi/2$ and the singular jump in $\bar{\varepsilon}_{\mathbf{k}}$ [see Eq. (79)] also disappears in agreement with the above assumption.

In a hypothetical case of the strong cubic term ($V_3\gg JS$) one needs to consider vertex renormalizations discussed in Appendix C. Briefly, this replaces the log singularity in the self-energy with $\mathrm{Im}\,\Sigma(\mathbf{k},\varepsilon)\propto 1/\ln|\Lambda/\rho|$. Solving the Dyson equation yield the same answer as in Eq. (82) for the $V_3^2/\Lambda(JS)^2\ll1$ limit, while in the opposite case solution for the single-particle spectrum near k^* does not exist. This is similar to the complete disappearance of the spectrum at the termination point of the spectrum in the superfluid ^{4}He.[46]

Finally, we present in Fig. 11 the numerical solution of the Dyson Eq. (77) for the spin-1/2 triangular lattice HAF. While the jumps and the logarithmic peaks disappear, the damping rate remains substantial throughout BZ. Note, that the overall shape of the off-shell $\bar{\varepsilon}_{\mathbf{k}}$ is in a better agreement with the series-expansion data[15] than the on-shell results. In particular, the "roton" minimum is well pronounced and the "flat regions" are much less significant than in the latter case. However, there is an overall upward energy scale offset of our results relative to the numerical ones. This may be due to both the remaining higher-order $1/S$ corrections to the spectrum in the spin-wave theory approach and the neglect of the imaginary part of the spectrum in the series-expansion calculations. The upward energy renormalization of the off-shell versus on-shell results is natural as the latter tends to overestimate the energy shifts.

Altogether, the main result of the off-shell consideration is that this approach naturally resolves the singularity problem, regularizing the log singularities in the decay rates and removing the concomitant jumplike discontinuities in the real part of the spectrum. As the result, the decay rates remain significant and are logarithmically enhanced relative to the perturbative results.

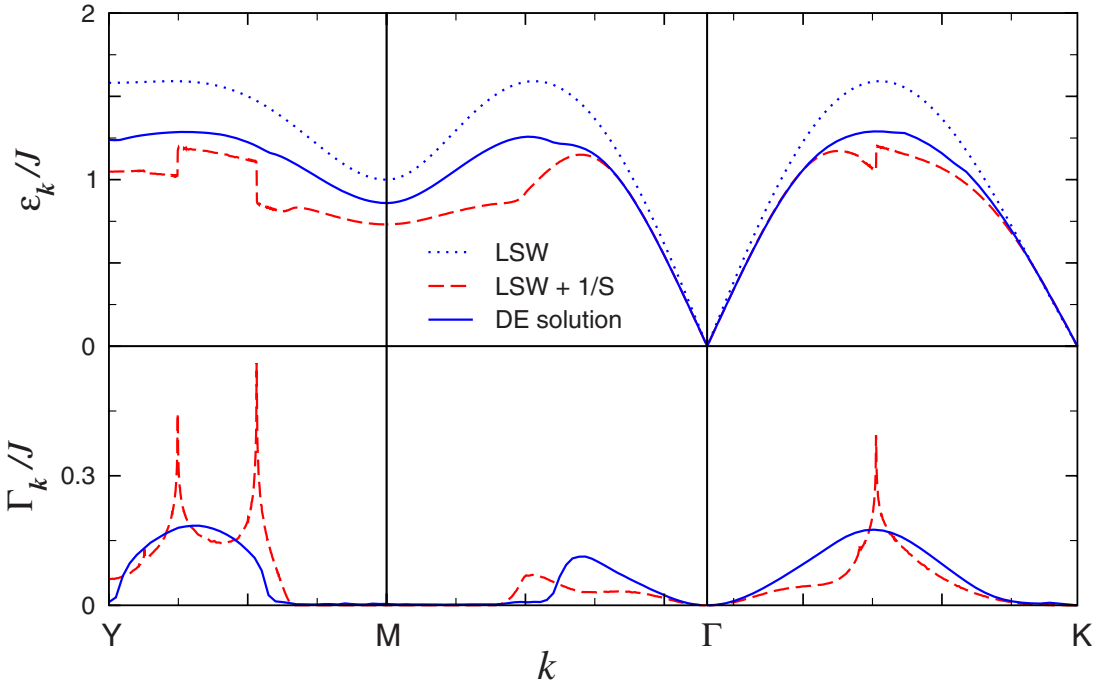

FIG. 11. (Color online) Comparison of the magnon spectrum (upper row) and the decay rates (lower row) obtained in the harmonic approximation (dotted lines), with the first-order $1/S$ corrections (dashed lines), and by solving the Dyson equation (solid lines), respectively.

B. Spectral function

Generally, a detailed information about both the polelike and the incoherent parts of the single-particle spectrum is obtained from the diagonal component of the spectral function

$$A(\mathbf{k},\omega) = -\frac{1}{\pi}\mathrm{Im}[G_{11}(\mathbf{k},\omega)]. \tag{85}$$

In the leading one-loop approximation the diagonal Green's function for the triangular lattice HAF is given by

$$G_{11}^{-1}(\mathbf{k},\omega) = \omega - \varepsilon_{\mathbf{k}} - \Sigma(\mathbf{k},\omega), \tag{86}$$

with $\Sigma(\mathbf{k},\omega)=\Sigma^{\mathrm{HF}}(\mathbf{k})+\Sigma_{11}^{(a)}(\mathbf{k},\omega)+\Sigma_{11}^{(b)}(\mathbf{k},\omega)$ expressed by Eq. (54). In quantum antiferromagnets the spectral function $A(\mathbf{k},\omega)$ is also related to the dynamical structure factor $S(\mathbf{k},\omega)$ which is directly measured in inelastic neutron experiments. Generally, $S(\mathbf{k},\omega)$ also has contributions from the off-diagonal and two-particle correlations,[33,40,41] but the spectral function (85) still provides the major component.

In the absence of intrinsic damping, the quasiparticle peak in $A(\mathbf{k},\omega)$ occurs precisely at $\omega=\bar{\varepsilon}_{\mathbf{k}}$ found from the solution of the Dyson equation. In the presence of spontaneous decays the solution of Eq. (77) differs from the position and the width of a quasiparticle peak in the spectral function because the latter is defined on the real ω axis. Another characteristic feature of $A(\mathbf{k},\omega)$ for all noncollinear AFs is the contribution from the two-magnon continuum due to a nonorthogonality of the one- and two-particle excitations. In particular, for the momenta $\mathbf{k}$ inside the decay region, the spectral weight in $A(\mathbf{k},\omega)$ should become nonzero above the bottom of the continuum. On the same ground, one should also expect singular behavior due to the van Hove singularities of the continuum to be prominent in the spectral function at any $\mathbf{k}$, not only at special contours of $\mathbf{k}^*$. This is because frequency scans through all possible energies and is not limited to the "mass surface" $\omega=\varepsilon_{\mathbf{k}}$. Since we are restricted to the one-loop approximation for $\Sigma(\mathbf{k},\omega)$ due to difficulties with the higher-order diagrams discussed above, such van Hove singularities will appear as sharp features in $A(\mathbf{k},\omega)$. This is due to both the one-loop approximation for the self-energy and because ω at which the system is probed is purely real. Qualitatively, all singularities are expected to be regularized by the higher-order contributions. The complication is, of course, that a quantitative calculation of such a regularization can be difficult if not impossible.

Figures 12 and 13 show the spectral function (85) for three different momenta: the M point (face center of the BZ) outside of the decay region and the two points on the ΓK line, $\mathbf{k}=(0.6085\pi,0)$ and $\mathbf{k}=(0.2\pi,0)$, both inside of the decay region. The momentum for Fig. 13(a) is $\mathbf{k}^*$, which corresponds to the logarithmic peak in the on-shell $\Gamma_{\mathbf{k}}$. The upper panels in Figs. 12 and 13 show the spectral function $A(\mathbf{k},\omega)$, while the lower panels contain $\mathrm{Re}\,G^{-1}(\mathbf{k},\omega)$, $\mathrm{Im}\,G^{-1}(\mathbf{k},\omega)$, and the two-magnon density of states (DoS)

$$D_{\mathbf{k}}^{2\mathrm{mag}}(\omega) = \sum_{\mathbf{q}} \delta(\omega - \varepsilon_{\mathbf{q}} - \varepsilon_{\mathbf{k}-\mathbf{q}}). \tag{87}$$

The energies of the noninteracting spin waves $\varepsilon_{\mathbf{k}}$ are indicated by dashed arrows. The quasiparticle peaks in $A(\mathbf{k},\omega)$ plots are marked by solid arrows. The lower panel shows that $\mathrm{Re}[G_{11}(\mathbf{k},\omega)^{-1}]$ vanishes at the same $\omega=\bar{\varepsilon}_{\mathbf{k}}$, as is expected for the pole behavior. For momenta inside the decay region, these peaks are also significantly broadened [see Figs. 13(a) and 13(b)]. While $\bar{\varepsilon}_{\mathbf{k}}$ differs very little from the one found in the numerical solution of the Dyson Eq. (77), the damping in

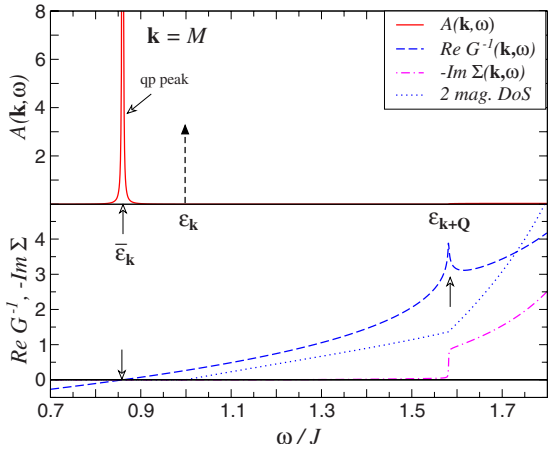

FIG. 12. (Color online) (Upper panel) Magnon spectral function $A(\mathbf{k},\omega)$ and (lower panel) real and imaginary parts of one-loop $G_{11}^{-1}(\mathbf{k},\omega)$ together with the two-magnon DoS (dotted line), all for $\mathbf{k}=(\pi,\pi/\sqrt{3})$ (M point). Dashed arrow in the upper panel indicates position of the "bare" magnon peak. Solid arrows denote position of the renormalized quasiparticle peak, zero of $\mathrm{Re}[G_{11}(\mathbf{k},\omega)^{-1}]$, and the van Hove singularities.

Figs. 13(a) and 13(b) is somewhat smaller than the one found self-consistently from Eq. (77). As we discuss in Appendix E, one can properly define the quasiparticle residue even for the case of the nonzero damping. The issue of defining it at a singularity point is also discussed there.

Confirming our previous discussion, the spectral weight in the decay region, Fig. 13, is nonzero above the two-magnon continuum ω boundary. The lower panels in Figs. 13(a) and 13(b) demonstrate that every singularity in the two-magnon DoS is reflected in both the real and the imaginary parts of the self-energy and, as a result, in the spectral function. For $\mathbf{k}=\mathbf{k}^*$ in Fig. 13(a) the bare magnon energy $\varepsilon_{\mathbf{k}}$ coincides with one such singularity, which corresponds to the decay into two magnons with energies $\varepsilon_{(\mathbf{k}+\mathbf{G}_3)/2}$. This intersection with the singularity surface causes the anomaly in the on-shell spectrum (see Sec. IV). For a nonsingular momentum in Fig. 13(b), which is not on the $\mathbf{k}^*$ contour, similar singularity is above the magnon energy.

Perhaps the most spectacular and also unexpected features of all the data in Figs. 13(a) and 13(b) are the sharp peaks at the bottom of the spectrum that *are not* associated with a concomitant peak in the two-magnon DoS. At the first glance, it may even be concluded that these peaks are the "true," well-defined quasiparticle peaks with zero damping. A close inspection of $\mathrm{Re}[\Sigma(\mathbf{k},\omega)]$ and $\mathrm{Im}[\Sigma(\mathbf{k},\omega)]$ in the lower panels clearly connects the peaks in $A(\mathbf{k},\omega)$ to the logarithmic and jumplike singularities in the one-loop self-energy. The origin of them is slightly more delicate than just a two-magnon DoS feature. The two-magnon DoS at the bottom of the continuum ε_b in the decay region corresponds to the boundary to the emission of the $\varepsilon_{\pm Q}$ magnon. Thus,with $\varepsilon_b=\varepsilon_{\mathbf{k}\pm\mathbf{Q}}$, $\Delta\omega=\varepsilon-\varepsilon_b$, and $\mathbf{q}$ in the vicinity of $\pm\mathbf{Q}$, the threshold behavior of it is

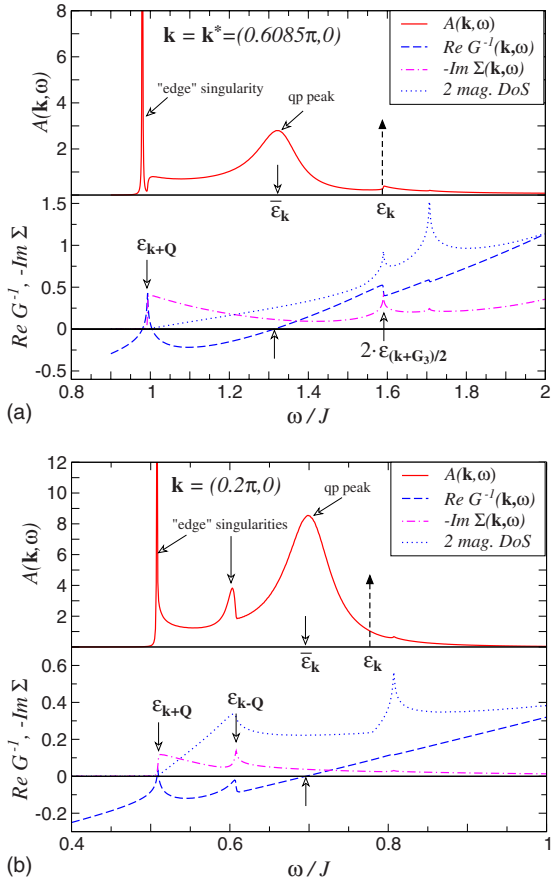

FIG. 13. (Color online) Same as in Fig. 12, for momenta on the ΓK line, (a) $\mathbf{k}=\mathbf{k}^*=\pi(0.6085,0)$ and (b) $\mathbf{k}=\pi(0.2,0)$. Solid vertical arrows indicate position of the quasiparticle peak, zero of $\mathrm{Re}[G_{11}^{-1}(\mathbf{k},\omega)]$, and van Hove and "edge" singularities (see text).

$$D_{\mathbf{k}}^{2\mathrm{mag}}(\omega)\propto\int qdq\,\delta(\Delta\omega-v_Q|\mathbf{q}|)\propto\Theta(\Delta\omega)(\Delta\omega). \quad (88)$$

Within the self-energy, the decay vertex exhibits anomalous behavior at small $\delta\mathbf{q}=\pm\mathbf{Q}+\mathbf{q}$ for $\mathbf{k}$ away from $\mathbf{k}=0$ and from the decay boundary $\tilde{\Gamma}_1(\mathbf{k},\mathbf{q})\propto 1/\sqrt{|\delta\mathbf{q}|}$. This yields a jumplike threshold behavior in the decay rate

$$\mathrm{Im}[\Sigma(\mathbf{k},\omega)]\propto\int dq\,\delta(\Delta\omega-v_Q|\mathbf{q}|)\propto\Theta(\Delta\omega) \quad (89)$$

and the concomitant log singularity in $\mathrm{Re}[\Sigma(\mathbf{k},\omega)]$ (as in Sec. V B). Thus, the weak threshold singularity of the type $\Theta(\Delta\omega)\Delta\omega$ in the two-magnon DoS is enhanced by the singular decay vertex. This leads to a zero in $\mathrm{Re}[G_{11}(\mathbf{k},\omega)^{-1}]$ and a "pseudo"-quasiparticle peak in $A(\mathbf{k},\omega)$. We refer to these anomalies in Figs. 13(a) and 13(b) as to the "edge" singularities. While in Fig. 13(a) this singularity is due to $\varepsilon_{-\mathbf{Q}}$ magnon, in Fig. 13(b) there are two such singularities: one associated with $\varepsilon_{-\mathbf{Q}}$ and the other $\varepsilon_{+\mathbf{Q}}$ magnon emission boundaries.

As is discussed earlier, all such singularities should be regularized by the higher-order treatment. For the "edge" singularities, the regularization requires summation of the

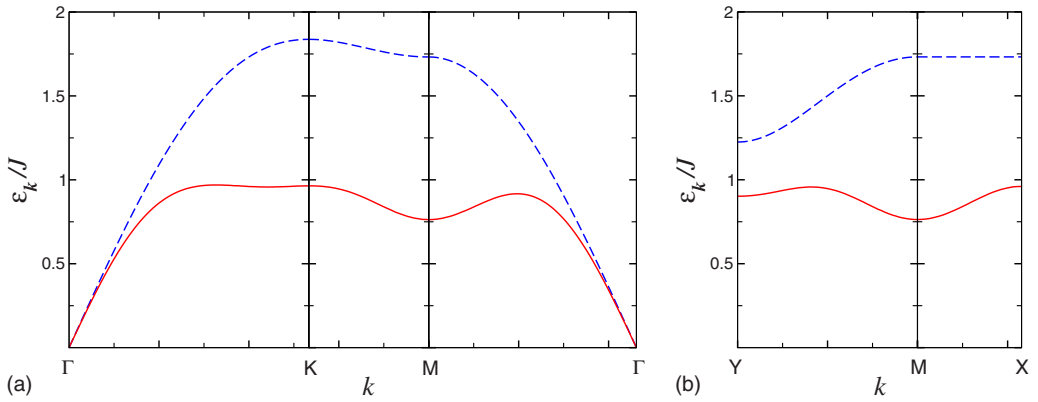

FIG. 14. (Color online) Magnon energy for the *XY* spin-1/2 triangular lattice AF along representative directions. Dashed line is the linear spin-wave dispersion and solid line is including the first $1/S$ correction.

Pitaevskii's sequence (see Appendix C) since the external energy is purely real in $A(\mathbf{k},\omega)$.

To summarize, the conventional consideration of the single-particle spectral function in the triangular lattice HAF is complicated by the logarithmic singularities associated with the van Hove singularities in the two-magnon continuum and with the singular behavior of the three-magnon coupling. Despite the contamination with these spurious features, a sensible analysis of the spectrum in terms of the broadened quasiparticle peak on the background of the two-magnon continuum is still possible.

VII. OTHER MODELS

In this section we demonstrate that anomalous features found in the spectrum of the triangular lattice Heisenberg antiferromagnet are generic and appear in a wide variety of noncollinear antiferromagnets. One straightforward generalization from the considered case is to the easy-plane *XXZ* model. Another modification consists of reducing lattice symmetry while keeping isotropic interaction between spins. This gives the so-called $J-J'$ model on an orthorhombically distorted triangular lattice: the Heisenberg exchange along horizontal chains J is stronger than the interchain coupling J'. Another system discussed here is the kagomé-lattice antiferromagnet with the *XXZ* anisotropy. In the following we outline basic kinematic conditions for two-magnon decays in these models and emphasize the singularities in the magnon spectrum.

A. *XXZ* model

The *XXZ* antiferromagnet on a triangular lattice is defined by the following Hamiltonian:

$$\hat{\mathcal{H}} = J\sum_{\langle ij\rangle}[S_i^x S_j^x + S_i^y S_j^y + \alpha S_i^z S_j^z]. \tag{90}$$

For the easy-plane system with the anisotropy parameter $\alpha = J_z/J < 1$ spins form the same 120° structure as in the Heisenberg case. In the harmonic approximation the spin-wave energy is given by a simple modification of the Heisenberg formula (13)

$$\varepsilon_{\mathbf{k}} = 3JS\sqrt{(1-\gamma_{\mathbf{k}})(1+2\alpha\gamma_{\mathbf{k}})}. \tag{91}$$

In addition, the three-boson interaction terms retain the same functional form as in Eqs. (19)–(22). Therefore, for the $1/S$ consideration of the *XXZ* model the changes concern only Bogolyubov parameters and quartic terms. While a detailed consideration of this model is beyond the scope of the present work, we would like to highlight two ubiquitous features of its spin-wave spectrum determined by the three-boson interactions: strong renormalizations and decays.

Let us first focus on the strongly anisotropic case and put $\alpha=0$. The ground-state energy for such an *XY* antiferromagnet is

$$E_{\mathrm{gs}}/N = -\frac{3}{2}JS^2\left[1 + \frac{0.064\,515}{2S} + \frac{0.013\,326}{(2S)^2}\right], \tag{92}$$

in agreement with Ref. 32. The harmonic spin-wave spectrum for this case is shown in Fig. 14 by dashed lines. Because of the reduced spin-rotational symmetry there is only one acoustic branch near the Γ point. The zero-point fluctuations reduce the sublattice magnetization to $\langle S\rangle = S - 0.051\,467$ in the linear spin-wave approximation. Even for the spin-1/2 case this amounts only to a 10% renormalization. Yet, the $1/S$ corrections to the spectrum shown by solid lines in Fig. 14 are even larger than in the isotropic case. Magnon bandwidth narrowing in $\alpha=0$ case is almost 50% of its bare value. One can also observe that the much-discussed rotonlike minimum at the *M* point is much more pronounced here than in the spin-wave results for the Heisenberg limit. The origin of this minimum can be traced to the one-dimensional (1D)-like van Hove singularity in the two-magnon density of states at the *M* point, similarly to the isotropic case (Sec. IV B). In addition, one can notice that the top of the renormalized magnon band exhibits much more extended flat regions than in the Heisenberg limit as well as some weaker minima (between Γ and *K*) and other extrema. These features must affect the thermodynamics of this model substantially. Thus, interpolating between $\alpha=0$ and $\alpha=1$ cases, one can conclude that the anharmonic three-boson terms lead to very strong spectrum renormalization throughout the BZ for the *XXZ* model on the triangular lattice for all values of α.

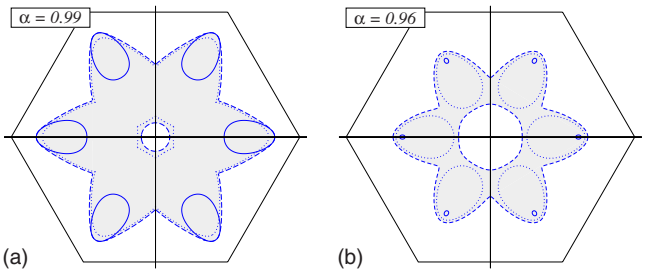

FIG. 15. (Color online) Decay region and singularity lines for the *XXZ* triangular lattice antiferromagnet with $\alpha=0.99$ (a) and $\alpha=0.96$ (b). Definition of lines is the same as in Fig. 9.

On the other hand, magnons in the $\alpha=0$ *XXZ* model are stable at $T=0$ and decays are absent. To study the evolution of the two-magnon decays we begin with the nearly Heisenberg limit $1-\alpha \ll 1$. Magnons with $\mathbf{q}=\pm\mathbf{Q}$ are gapped with $\varepsilon_{\mathbf{Q}}=\sqrt{3(1-\alpha)/2}$. This has two immediate consequences in comparison to the $\alpha=1$ limit: (a) magnons at $\mathbf{k}\to 0$ cannot decay into two $\varepsilon_{\mathbf{Q}}$ magnons up to $\mathbf{k}$ values such that $\varepsilon_{\mathbf{k}}=2\varepsilon_{\mathbf{Q}}$ and (b) $\mathbf{Q}$ magnons become stable themselves for the same reason. As a result, the star-shaped decay region of Fig. 9 develops a hole in the middle and has vertices shrunk and rounded (see Fig. 15). The evolution of the character of the decay boundary with α is nontrivial. Initially, the emission of a $\mathbf{Q}$ magnon remains an absolute minimum of the two-magnon continuum for most of the decay region except the tips of the star vertices. At $\alpha_1\approx 0.993$ the decay into a pair of nonequivalent magnons switches from being a line of saddle points into the absolute minima of the continuum and takes over the decay boundary (compare dotted and dashed lines in Figs. 9 and 15). Without going into details, we simply note that in such a case the real part of the spectrum is singular, $\mathrm{Re}\,\Sigma(k_b,\omega)\propto \ln|k-k_b|$ [see Eq. (75)] which is similar to the case of excitations in ^{4}He near the threshold of decay into a pair of rotons.[29,46] Similarly to the latter case, finding the spectrum near the boundary will require summation of the higher-order diagrams. Figure 15 shows the evolution of the decay region and singularity lines between $\alpha=0.99$ and $\alpha=0.96$. Further decrease of α completely eliminates the decay region at around $\alpha\approx 0.92$. Therefore, magnon decays are present in an anisotropic triangular lattice AFs, but only for not very strong anisotropies.

B. $J-J'$ model

Another variety of generalizations of the nearest-neighbor Heisenberg model can be generated by spatial anisotropies, keeping spin-space intact. A particular model of this type corresponds to an orthorhombically distorted triangular lattice

$$\hat{\mathcal{H}}=J\sum_{\langle ij\rangle}^{x}\mathbf{S}_i\cdot\mathbf{S}_j+J'\sum_{\langle ij\rangle}^{\text{z-z}}\mathbf{S}_i\cdot\mathbf{S}_j, \tag{93}$$

in which interactions along the "1D chains" running parallel to the x axis is J, while zig-zag interaction between the chains is J'. This model has attracted a lot of attention due to experimentally available systems, Cs_2CuCl_4 (Ref. 2) and Cs_2CuBr_4,[47] with J'/J is ≈ 0.34 and ≈ 0.7, respectively. For the former system, a comprehensive experimental neutron-scattering analysis of the spin-excitation spectrum has been performed[2] and an extensive theoretical analysis using both the spin-wave theory and the 1D spinon-based approach have been carried out.[41,40,48,49] We do not intend to repeat any of these calculations here, but would like to emphasize that a substantial broadening of the spin waves in a major part of the BZ must persist throughout the phase diagram of the $J-J'$ model.

The ground state of the classical $J-J'$ model is an incommensurate spin spiral. In the harmonic approximation, the energy of the spin waves in the $J-J'$ model with $J'/J<2$ is[41]

$$\varepsilon_{\mathbf{k}}=6SJ\sqrt{(\gamma_{\mathbf{k}}-\gamma_{\mathbf{Q}})[(\gamma_{\mathbf{Q}+\mathbf{k}}+\gamma_{\mathbf{Q}-\mathbf{k}})/2-\gamma_{\mathbf{Q}}]}, \tag{94}$$

where

$$\gamma_{\mathbf{k}}=\frac{1}{3}\left(\cos k_x+2\frac{J'}{J}\cos\frac{k_x}{2}\cos\frac{\sqrt{3}k_y}{2}\right) \tag{95}$$

and the ordering vector $\mathbf{Q}=(Q_x,0)$ is given by

$$Q_x=\pi+2\arcsin(J'/2J). \tag{96}$$

Since the $SO(3)$ symmetry is preserved in the $J-J'$ model, the Goldstone modes remain at $\mathbf{k}=0$ and $\mathbf{k}=\pm\mathbf{Q}$ points with the incommensurate ordering wave vector $\mathbf{Q}$ [Eq. (96)]. Thus, because the velocities of these modes must generally stay different, magnon decays will always be allowed. In Fig. 16 we show the 3D shape of the linear spin-wave energy for $J'/J=0.34$. All notations and symmetry points are the same as in Fig. 2, k_x is in units of $1/a$, and k_y is in units of $1/b$, where a and b are the lattice constants in the chain and interchain directions, respectively. One can observe a more sophisticated shape of the dispersion with three saddle points at different energies (M, M', and between M' and K' points). Comparing this figure with the $J=J'$ case of Fig. 2 one also finds that with the decrease of J' the spin-wave spectrum develops a low-energy branch in the y direction (between the chains with strong J). That should make the rest of the spectrum prone to decays into it.

To analyze the decays on a more qualitative level we show the decay regions and the singularity lines for two representative values of J'/J in Fig. 16. First, the boundary of the decay region is determined by the emission of the gapless $\pm\mathbf{Q}$ magnon for any value of J'/J as in the $J'=J$ case. Second, the incommensurability of the ordering wave vector $\mathbf{Q}$ does not change the kinematics of the decays near $\mathbf{k}\to 0$ where the spin-waves can always decay into two modes near $+\mathbf{Q}$ and $-\mathbf{Q}$. However, the incommensurability forbids the decays from near the $\mathbf{Q}$ point into the vicinity of $-\mathbf{Q}$ point since the $2\mathbf{Q}$ wave vector is not equal to any reciprocal-lattice vector anymore and quasimomentum cannot be conserved in such a decay. This leads to shrinking of the vertices of the star-shaped decay region in the k_x direction (see Fig. 16). However, the vertices expand considerably in the k_y direction. The singularity lines due to the saddle points in the two-magnon continuum also expand and stretch in the k_y direction as J' is lowered, in agreement with the expectations

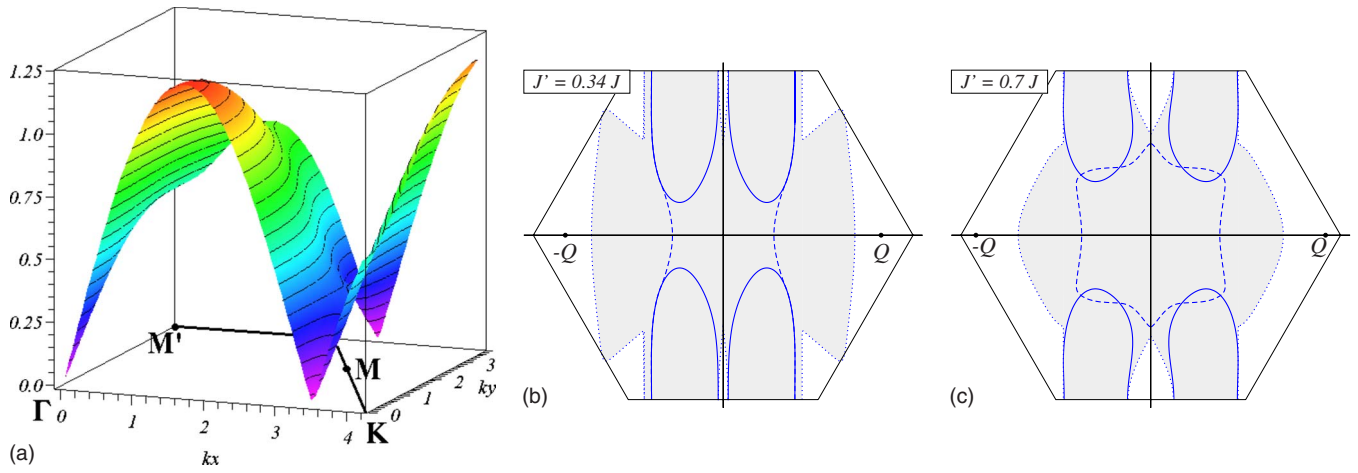

FIG. 16. (Color online) Left panel: the 3D shape of the linear spin-wave frequency $\omega_{\mathbf{k}}=\varepsilon_{\mathbf{k}}/2JS$ for the $J-J'$ antiferromagnet with $J'/J=0.34$. Central panel: the decay region and the singularity lines at $J'/J=0.34$ (definitions are the same as in Fig. 9). Right panel: same for $J'/J=0.7$.

from the shape of the dispersion. Overall, the decay region grows with the decrease of J'. At $J'\approx 0.34J$, relevant to Cs_2CuCl_4,[2] the decay region covers most of the BZ [see Fig. 16].

Within the spin-wave theory, a significant phase-space volume for the decays found at $J'/J=0.34$ can be somewhat compensated by smaller noncollinearity of the spins which reduces the decay amplitudes. In real Cs_2CuCl_4, additional Dzyaloshinskii-Moriya interactions make this angle large (close to 90°) between the spins in the nearest-neighbor 1D chains,[2] but almost antiparallel within the individual chains with strong J. This means that, effectively, the decay vertices are proportional to the weaker coupling J'. However, the decays of the spin-waves still result in a substantial damping (see Refs. 41 and 40). Altogether, the $J-J'$ model should exhibit magnon decays and singularities in their spin-wave spectrum throughout all the ranges of J' where the spin-wave theory is applicable.

C. *XXZ* model on the kagomé lattice

The Heisenberg antiferromagnet on the kagomé lattice is magnetically disordered at $T=0$ in both the classical ($S=\infty$) and the $S=1/2$ limits.[50–52] The degeneracy of the classical ground state reveals itself in the presence of the dispersionless zero-energy branch of magnons in the harmonic spectrum. The easy-plane anisotropy does not lift such a degeneracy, while opening up a constant gap for the zero-energy mode. A somewhat different behavior is realized in the recently discovered kagomé-lattice compound potassium jarosite.[53] In this antiferromagnet, the Dzyaloshinskii-Moriya interactions lift the zero-energy mode to finite energies removing simultaneously the classical degeneracy in favor of a so-called $\mathbf{q}=0$ spin configuration. Still, the easy-plane *XXZ* model,

$$\hat{\mathcal{H}}=J\sum_{\langle ij\rangle}[S_i^xS_j^x+S_i^yS_j^y+\alpha S_i^zS_j^z], \tag{97}$$

is more advantageous for a qualitative consideration of the magnon spectrum because analytic expressions for the spin-wave energies can be easily derived.

Since the unit cell of the kagomé lattice consists of three atoms, there are three branches of magnetic excitations. For the 120° structure, the energies of these branches in the harmonic approximation are given by

$$\varepsilon_{\mathbf{k}}^{(i)}=2JS\omega_{\mathbf{k}}^{(i)}, \tag{98}$$

where

$$\omega_{\mathbf{k}}^{(1)}=\sqrt{\frac{3}{2}}\sqrt{1-\alpha}=\omega_0,$$

$$\omega_{\mathbf{k}}^{(2,3)}=\sqrt{1-\alpha\gamma_{\mathbf{k}}-\frac{(1-\alpha)}{4}(1\pm\sqrt{1+8\gamma_{\mathbf{k}}})}, \tag{99}$$

with

$$\gamma_{\mathbf{k}}=\cos k_1\cos k_2\cos k_3, \tag{100}$$

and $k_1=k_x$, $k_{2,3}=\pm k_x/2+k_y\sqrt{3}/2$, respectively. Thus, there is a gapped dispersionless mode, ω_0, gapped dispersive one, $\omega_{\mathbf{k}}^{(2)}$, and gapless one, $\omega_{\mathbf{k}}^{(3)}$ (see Fig. 17 where $\omega_{\mathbf{k}}^{(i)}$ are shown for $\alpha=0.95$). In the real system, the lowest branch is weakly dispersive.[53] Using symmetry consideration, the BZ for the kagomé-lattice HAF can be reduced to the one smaller than the triangular lattice BZ (see Ref. 51). In Fig. 17, ΓXY cuts are according to the notations of this work, with $X=(0,2\pi/3)$ and $Y=(\pi/2,\pi/2\sqrt{3})$.

Since the three modes in (99) are some linear combinations of local spin-flips, the three-boson interaction due to noncollinearity of the spin structure will necessarily facilitate couplings of all three branches with each other. Such a coupling should not have any apparent smallness aside from the $1/\sqrt{S}$ factor, same as in Eq. (20). Therefore, some qualitative conclusions about magnon decays in this system can be made without the detailed technical analysis.

A distinct feature of the spin waves in the kagomé AFs is a (almost) dispersionless mode. For the decays this means that in the decays involving one of such magnons the momentum conservation can be ignored. This immediately implies that any spin wave with the energy exceeding ω_0 will

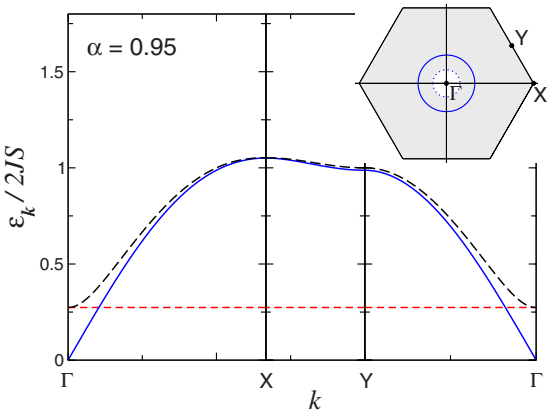

FIG. 17. (Color online) Linear spin-wave frequencies of the excitations in the *XXZ* model on the kagomé lattice, Eq. (99) for $\alpha=0.95$, along ΓXY cuts. Notations for the BZ are the same as in Ref. 51. Lines and shaded area are the decay boundary (dotted), strong singularity line (solid), and the decay region, respectively (see text).

have a finite lifetime due to decays into one ω_0 magnon and a Goldstone mode of the gapless branch. Thus, all the excitations above the horizontal dashed line in Fig. 17 will be damped due to such decays. Another observation is that there must exist a particularly strong singularity in both dispersive branches $\omega_{\mathbf{k}}^{(2)}$ and $\omega_{\mathbf{k}}^{(3)}$ at the energy twice the energy of the dispersionless mode. This is because the self-energy near $2\omega_0$ will have a resonantlike form $\Sigma_{\mathbf{k}}(\omega) \propto |V|^2/(\omega-2\omega_0)$. Even for the case when the lower branch has some residual dispersion, the damping of $\omega_{\mathbf{k}}^{(2,3)}$ must be anomalously large near $2\omega_0$ in comparison to the rest of the spectrum. This should be valid even for large values of spin and in both 2D and 3D systems. Such a singularity is much stronger than the logarithmic singularities discussed in the rest of this paper and should be readily observed in experiment.

D. Summary of Sec. VII

Summarizing the above examples, we conclude that strong renormalization, significant damping, and singularities must be common features of the excitation spectra of a wide variety of noncollinear AFs. The enhancement of damping along certain contours due to singularities should be considered as fingerprints of magnon decays. This should help to distinguish the decay-induced spin-wave broadening from the other scenarios that yield broad spectra of the spin excitations.

VIII. CONCLUSIONS

To summarize, the triangular lattice AF is a prominent example of a geometrically frustrated magnetic system. Present study has demonstrated that the frustration-induced noncollinearity of the spin structure in such systems is both the source and the key to understanding of their anomalous spin-wave spectra. The highlights of the anomalous features of the spectrum that should be observable in experiments are the substantial broadening of magnon peaks due to spontaneous decays in a large part of the Brillouin zone and strong deviations of the spectrum from the LSWT expectations for $S=1/2$ systems. The broadening should also be enhanced by the $\ln S$ factor in the vicinity of certain contours in the momentum space due to the van Hove singularities in the two-magnon continuum. Such an enhancement might be more visible in the systems with larger spins, such as the spin-5/2 triangular lattice $RbFe(MoO_4)_2$,[3] although the overall damping will be smaller due to the $1/S$ effect. As the measurements of the lifetimes of spin excitations in the neutron-scattering experiments are expected to improve drastically in the future,[57] this will allow for the detailed analysis of the damping. Therefore, the enhancement of the damping along specific contours will be able to serve as a fingerprint of the spin-wave decays and could help to distinguish the spin-wave decay mechanism from the other scenarios such as fractionalization of spin excitations into spinons.[49,58] We have also demonstrated that the strong renormalization, decays, and singularities in the spectrum are prominent in a wide variety of frustrated AFs of current interest.

The strong cubic anharmonic coupling of the spin-waves induced by the noncollinearity is also the source of various technical challenges within the spin-wave approach. Such challenges are largely unfamiliar in the well-studied bipartite (collinear) AFs where interactions are weaker and are of higher order. In this work, we have demonstrated that the spin-wave theory encounters some new problems in treating magnon interactions in the noncollinear AFs. Generally speaking, the standard $1/S$ expansion for the spectrum becomes nonanalytic, which is manifested by the singularities in the first-order $1/S$ self-energy. The origin of such singularities is related to the crossing of the single-particle branch with the surface of van Hove singularities in the two-magnon continuum. Regularization of such singularities also requires extra technical effort of going beyond the lowest-order $1/S$ approximation.

ACKNOWLEDGMENTS

We are grateful to O. Starykh and A. Chubukov for illuminating discussions. We also thank H. Tsunetsugu for bringing Ref. 8 to our attention. Part of this work has been done at the Max Planck Institute for the Physics of Complex Systems, which we would like to thank for hospitality. This work was supported by DOE under Grant No. DE-FG02-04ER46174 (A.L.C.). The research at KITP was supported by the NSF under Grant No. PHY05-51164 (A.L.C.).

APPENDIX A: HARTREE-FOCK CORRECTIONS

In the harmonic approximation the following Hartree-Fock averages are nonzero for the triangular lattice HAF:

$$n = \langle a_i^\dagger a_i \rangle = \sum_{\mathbf{k}} v_{\mathbf{k}}^2 = \frac{1}{2}\sum_{\mathbf{k}} \frac{1+\frac{1}{2}\gamma_{\mathbf{k}}}{\omega_{\mathbf{k}}} - \frac{1}{2},$$

$$m = \langle a_i^\dagger a_j \rangle = \sum_{\mathbf{k}} \gamma_{\mathbf{k}} v_{\mathbf{k}}^2 = \frac{1}{2}\sum_{\mathbf{k}} \frac{\gamma_{\mathbf{k}}+\frac{1}{2}\gamma_{\mathbf{k}}^2}{\omega_{\mathbf{k}}},$$

$$\Delta = \langle a_i a_j \rangle = \sum_{\mathbf{k}} \gamma_{\mathbf{k}} u_{\mathbf{k}} v_{\mathbf{k}} = \frac{3}{4} \sum_{\mathbf{k}} \frac{\gamma_{\mathbf{k}}^2}{\omega_{\mathbf{k}}},$$

$$\delta = \langle a_i^2 \rangle = \sum_{\mathbf{k}} u_{\mathbf{k}} v_{\mathbf{k}} = \frac{3}{4} \sum_{\mathbf{k}} \frac{\gamma_{\mathbf{k}}}{\omega_{\mathbf{k}}}. \tag{A1}$$

These four constants can be expressed through combinations of three two-dimensional integrals

$$c_l = \sum_{\mathbf{k}} \frac{(\gamma_{\mathbf{k}})^l}{\omega_{\mathbf{k}}}, \quad c_0 = 1.574\ 733\ 4,$$

$$c_1 = -0.104\ 253\ 9, \quad c_2 = 0.344\ 445\ 8. \tag{A2}$$

As is discussed in Sec. III A 3, the quartic terms (24) yield a correction to the ground-state energy that is given by the four-boson averages. In the leading order, they can be decoupled into the bilinear combinations (A1) using the Wick's theorem. The corresponding terms in Eq. (24) are given by

$$\langle a_i^\dagger a_i a_j^\dagger a_j \rangle = n^2 + m^2 + \Delta^2,$$

$$\langle a_i^\dagger a_i a_i a_j \rangle = 2n\Delta + m\delta, \quad \langle a_j^\dagger a_j^\dagger a_j a_i \rangle = 2nm + \Delta\delta. \tag{A3}$$

This yields the ground-state energy correction from the quartic terms

$$\delta E_4 = -\frac{3}{2} J \left[n^2 + m^2 + \Delta^2 - 3n\Delta - \frac{3}{2} m\delta + nm + \frac{1}{2} \Delta\delta \right]. \tag{A4}$$

After some further algebra the above expression is converted into a combination of c_l constants given by Eq. (26).

A similar mean-field decoupling procedure yields the following correction to the harmonic part of the Hamiltonian in terms of the original bosons:

$$\delta\tilde{\mathcal{H}}_2 = \sum_{\mathbf{k}} \delta A_{\mathbf{k}} a_{\mathbf{k}}^\dagger a_{\mathbf{k}} - \frac{1}{2} \delta B_{\mathbf{k}} (a_{\mathbf{k}} a_{-\mathbf{k}} + a_{-\mathbf{k}}^\dagger a_{\mathbf{k}}^\dagger),$$

$$\delta A_{\mathbf{k}} = -\frac{3}{4} J \left[2(c_0 + c_1 - 2c_2 - 1) + \gamma_{\mathbf{k}} \left(c_0 + c_2 - 1 + \frac{1}{4} c_1 \right) \right],$$

$$\delta B_{\mathbf{k}} = \frac{9}{4} J \left[\gamma_{\mathbf{k}} \left(1 + c_2 - c_0 - \frac{1}{4} c_1 \right) - \frac{1}{2} c_1 \right]. \tag{A5}$$

After that one uses the Bogolyubov transformation (9) and obtains the following quadratic form of magnon operators:

$$\delta\tilde{\mathcal{H}}_2 = \sum_{\mathbf{k}} \varepsilon_{\mathbf{k}}^{(4)} b_{\mathbf{k}}^\dagger b_{\mathbf{k}} - \frac{1}{2} B_{\mathbf{k}}^{(4)} (b_{\mathbf{k}} b_{-\mathbf{k}} + b_{-\mathbf{k}}^\dagger b_{\mathbf{k}}^\dagger). \tag{A6}$$

The coefficients in this expression are related to $\delta A_{\mathbf{k}}$ and $\delta B_{\mathbf{k}}$ by

$$\varepsilon_{\mathbf{k}}^{(4)} = (u_{\mathbf{k}}^2 + v_{\mathbf{k}}^2) \delta A_{\mathbf{k}} - 2u_{\mathbf{k}} v_{\mathbf{k}} \delta B_{\mathbf{k}},$$

$$B_{\mathbf{k}}^{(4)} = (u_{\mathbf{k}}^2 + v_{\mathbf{k}}^2) \delta B_{\mathbf{k}} - 2u_{\mathbf{k}} v_{\mathbf{k}} \delta A_{\mathbf{k}}, \tag{A7}$$

which lead finally to Eqs. (28) and (29).

APPENDIX B: SUBLATTICE MAGNETIZATION

Calculation of the second-order correction to the sublattice magnetization (46) requires evaluation of the lowest-order contributions to $\langle b_{\mathbf{k}}^\dagger b_{\mathbf{k}} \rangle$ and $\langle b_{\mathbf{k}} b_{-\mathbf{k}} \rangle$, which are expressed in terms of the normal and the anomalous Green's functions, respectively,

$$\langle b_{\mathbf{k}}^\dagger b_{\mathbf{k}} \rangle = i \int \frac{d\omega}{2\pi} G_{11}(\mathbf{k}, \omega) e^{i\omega\delta},$$

$$\langle b_{\mathbf{k}} b_{-\mathbf{k}} \rangle = i \int \frac{d\omega}{2\pi} G_{12}(\mathbf{k}, \omega). \tag{B1}$$

One needs to keep only the first-order terms in the perturbative expansion of the Green's functions. The diagonal average $\langle b_{\mathbf{k}}^\dagger b_{\mathbf{k}} \rangle$ has a single nonzero contribution determined by $\delta G_{11}(\mathbf{k}, \omega) = G_0^2(\mathbf{k}, \omega) \Sigma_{11}^{(b)}(\mathbf{k}, \omega)$,

$$\langle b_{\mathbf{k}}^\dagger b_{\mathbf{k}} \rangle = \frac{1}{2} \sum_{\mathbf{q}} \frac{|\Gamma_2(\mathbf{q};\mathbf{k})|^2}{(\varepsilon_{\mathbf{k}} + \varepsilon_{\mathbf{q}} + \varepsilon_{\mathbf{k}+\mathbf{q}})^2}, \tag{B2}$$

which yields

$$\delta S_{2,1} = \frac{3}{4S} \sum_{\mathbf{k},\mathbf{q}} \frac{1 + \frac{1}{2}\gamma_{\mathbf{k}}}{\omega_{\mathbf{k}}} \frac{\tilde{\Gamma}_2(\mathbf{q};\mathbf{k})^2}{(\omega_{\mathbf{k}} + \omega_{\mathbf{q}} + \omega_{\mathbf{k}+\mathbf{q}})^2}, \tag{B3}$$

where we have transformed to the dimensionless vertex and frequencies in the last expression.

The off-diagonal average $\langle b_{\mathbf{k}} b_{-\mathbf{k}} \rangle$ is determined by the lowest-order anomalous self-energies

$$\delta G_{12}(\mathbf{k}, \omega) = G_0(\mathbf{k}, \omega) G_0(-\mathbf{k}, -\omega) \Sigma_{12}(\mathbf{k}, \omega), \tag{B4}$$

with $\Sigma_{12}(\mathbf{k}, \omega) = \Sigma_{\mathrm{HF}}(\mathbf{k}) + \Sigma_{12}^{(c)}(\mathbf{k}, \omega) + \Sigma_{12}^{(d)}(\mathbf{k}, \omega)$. The first frequency-independent contribution from the Hartree-Fock self-energy (37) yields

$$\delta S'_{2,2} = -\frac{9}{16S} \sum_{\mathbf{k}} \frac{\gamma_{\mathbf{k}}(1 - \gamma_{\mathbf{k}})}{\omega_{\mathbf{k}}^3} \left(\frac{1}{2} c_1 + c_2 \gamma_{\mathbf{k}} \right)$$

$$= -\frac{9}{32S} c_1 c_2 + \frac{9}{32S} (c_2 - c_1) \sum_{\mathbf{k}} \frac{\gamma_{\mathbf{k}}(1 - \gamma_{\mathbf{k}})}{\omega_{\mathbf{k}}^3}. \tag{B5}$$

Two other terms give identical contributions to $\langle b_{\mathbf{k}} b_{-\mathbf{k}} \rangle$ with the net result

$$\delta S''_{2,2} = \frac{9}{8S} \sum_{\mathbf{k}} \frac{\gamma_{\mathbf{k}}}{\omega_{\mathbf{k}}^2} \sum_{\mathbf{q}} \frac{\tilde{\Gamma}_1(\mathbf{q};\mathbf{k}) \tilde{\Gamma}_2(\mathbf{q};\mathbf{k})}{\omega_{\mathbf{k}} + \omega_{\mathbf{q}} + \omega_{\mathbf{k}-\mathbf{q}}}. \tag{B6}$$

Combining all of the above terms together, we obtain

$$\delta S_2 = -\frac{9}{16} c_1 c_2 + \frac{9}{16} (c_2 - c_1) \sum_{\mathbf{k}} \frac{\gamma_{\mathbf{k}}(1 - \gamma_{\mathbf{k}})}{\omega_{\mathbf{k}}^3}$$

$$+ \frac{9}{4} \sum_{\mathbf{k}} \frac{\gamma_{\mathbf{k}}}{\omega_{\mathbf{k}}^2} \sum_{\mathbf{q}} \frac{\tilde{\Gamma}_1(\mathbf{k},\mathbf{q}) \tilde{\Gamma}_2(-\mathbf{k},\mathbf{q})}{\omega_{\mathbf{q}} + \omega_{\mathbf{k}-\mathbf{q}} + \omega_{\mathbf{k}}}$$

$$+ \frac{3}{2} \sum_{\mathbf{k}} \frac{1 + \frac{1}{2}\gamma_{\mathbf{k}}}{\omega_{\mathbf{k}}} \sum_{\mathbf{q}} \frac{\tilde{\Gamma}_2(\mathbf{k},\mathbf{q})^2}{(\omega_{\mathbf{q}} + \omega_{\mathbf{k}+\mathbf{q}} + \omega_{\mathbf{k}})^2}. \tag{B7}$$

As discussed in Sec. III B 2, one cannot use Eq. (B7) for numerical evaluation of δS_2 directly as it leads to ambiguous results or simply does not converge. The way to regularize the above expression is to use an analytical insight.[11] The integrand in the third term in (B7) can be reduced precisely to the divergent second term for $\mathbf{k}\to\mathbf{Q}$,

$$\frac{9}{4}\frac{\gamma_{\mathbf{k}}}{\omega_{\mathbf{k}}^2}\sum_{\mathbf{q}}\left.\frac{\tilde{\Gamma}_1(\mathbf{k},\mathbf{q})\tilde{\Gamma}_2(-\mathbf{k},\mathbf{q})}{\omega_{\mathbf{q}}+\omega_{\mathbf{k}-\mathbf{q}}+\omega_{\mathbf{k}}}\right|_{\mathbf{k}\to\mathbf{Q}} = -\frac{9}{16}(c_2-c_1)\frac{\gamma_{\mathbf{k}}(1-\gamma_{\mathbf{k}})}{\omega_{\mathbf{k}}^3}+\mathcal{O}(\omega_{\mathbf{k}}^{-2}). \tag{B8}$$

Then, the proper subtraction of the leading singularities is ensured by re-expressing the *second* term in Eq. (B7) as a double integral over $\mathbf{k}$ and $\mathbf{q}$ using Eq. (B8). An additional technical detail is that one should use projector-type multipliers $P_1=\frac{2}{3}(1-\gamma_{\mathbf{k}})$ and $P_2=\frac{1}{3}(1+2\gamma_{\mathbf{k}})$ to avoid introducing extra singularities by the above conversion in the second term. These projectors obey $P_1+P_2=1$ and guarantee convergence of the integrals close to the $\mathbf{k}=0$ and $\mathbf{k}=\mathbf{Q}$ points, respectively. Altogether, this has led us to the analytically identical, but numerically regular form of the $1/S^2$ correction to the on-site magnetization

$$\delta S_2 = -\frac{9}{16}c_1c_2+\delta\hat{S}^{3,1}+\delta\hat{S}^{3,2}+\delta\hat{S}^{3,3}, \tag{B9}$$

where the second and third terms are regular from the start due to projectors and the last term is the regularized combination of all singular terms. Specifically

$$\delta\hat{S}^{3,1}=\sum_{\mathbf{k}}\frac{\left(1+\frac{1}{2}\gamma_{\mathbf{k}}\right)}{\omega_{\mathbf{k}}}\left(\frac{1}{2}+\gamma_{\mathbf{k}}\right)\sum_{\mathbf{q}}\frac{\tilde{\Gamma}_2(\mathbf{k},\mathbf{q})^2}{(\omega_{\mathbf{q}}+\omega_{\mathbf{k}+\mathbf{q}}+\omega_{\mathbf{k}})^2},$$

$$\delta\hat{S}^{3,2}=\frac{3}{4}\sum_{\mathbf{k}}\frac{\gamma_{\mathbf{k}}}{\omega_{\mathbf{k}}^2}(1+2\gamma_{\mathbf{k}})\sum_{\mathbf{q}}\frac{\tilde{\Gamma}_1(\mathbf{k},\mathbf{k}-\mathbf{q})\tilde{\Gamma}_2(-\mathbf{k},\mathbf{q})}{\omega_{\mathbf{q}}+\omega_{\mathbf{k}-\mathbf{q}}+\omega_{\mathbf{k}}}.$$

The combination of the divergent terms is given by

$$\delta\hat{S}^{3,3}=\frac{3}{2}\sum_{\mathbf{k}}\frac{(1-\gamma_{\mathbf{k}})}{\omega_{\mathbf{k}}^2}\sum_{\mathbf{q}}\left[\gamma_{\mathbf{k}}\left(\frac{\tilde{\Gamma}_1(\mathbf{k},\mathbf{k}-\mathbf{q})\tilde{\Gamma}_2(-\mathbf{k},\mathbf{q})}{\omega_{\mathbf{q}}+\omega_{\mathbf{k}-\mathbf{q}}+\omega_{\mathbf{k}}}-\frac{\tilde{\Gamma}_1(\mathbf{Q},\mathbf{Q}-\mathbf{q})\tilde{\Gamma}_2(-\mathbf{Q},\mathbf{q})}{\omega_{\mathbf{q}}+\omega_{\mathbf{Q}-\mathbf{q}}}\right)+\frac{2}{3}\frac{\omega_{\mathbf{k}}\left(1+\frac{1}{2}\gamma_{\mathbf{k}}\right)\tilde{\Gamma}_2(\mathbf{k},\mathbf{q})^2}{(\omega_{\mathbf{q}}+\omega_{\mathbf{k}+\mathbf{q}}+\omega_{\mathbf{k}})^2}\right].$$

The results of the numerical integration of the individual terms are

$$-\frac{9}{16}c_1c_2=0.201\ 992\ 72,\quad \delta\hat{S}^{3,1}=0.017\ 918(1),$$

$$\delta\hat{S}^{3,2}=0.025\ 496(2),\quad \delta\hat{S}^{3,3}=-0.074\ 660(5).$$

Altogether, they lead to the following value of the second-order correction:

$$\delta S_2=-0.011\ 045(5). \tag{B10}$$

APPENDIX C: HIGHER-ORDER SINGULARITIES

Singularities in the perturbative calculations of the bosonic excitation spectra are known since the early works by Pitaevskii[29,46] on the termination point in the phonon branch of ^{4}He. There is a renewed interest in the similar problems in the context of various spin systems.[30] On the other hand, the logarithmic singularities in the fermionic spectra are also known to occur since the early works on the edge-singularities in metals,[54] in the context of numerous aspects of 1D Luttinger liquids,[55] as well as in the newer physical systems such as graphene.[56]

In all these problems, some physical processes, often of a threshold nature, lead to a nonanalytic behavior of various quantities. Such a nonanalyticity manifests itself in a breakdown of the perturbative expansion, i.e., as a singularity. The theoretical challenge is to reconstruct the original nonanalytic behavior from the singular terms in the perturbative expansion. In the Pitaevskii's case, such a reconstruction is rather straightforward and consists of resummation of the leading divergent terms of the "ladder" (random-phase approximation, RPA) type. In such a case, the original nonanalyticity is straightforwardly related to the singularity, e.g., $1/\ln|\omega|$ to $\ln|\omega|$, respectively. In the fermionic systems, such a resummation is more complicated and involves the infamous "parquet" diagrams. However, often enough, the reconstruction of the original nonanalytic behavior is still possible from the analysis of a few most-divergent terms of the expansion. In some well-known cases, the log singularity resumes in a nonanalyticity of a nontrivial fractional power-law type, $|\omega|^{\alpha}$.[54]

Since in our case we deal with bosonic excitations, one can expect that the Pitaevskii's consideration is the most relevant one. While this expectation, with some minor corrections, turns out to be true, we would like to outline some differences and similarities of the singularities in the spectra of noncollinear AFs in a somewhat broader context.

One obvious difference of our problem from the fermionic case is the presence of two coupling constants, three-particle, V_3, and four-particle, V_4, depicted in Fig. 3. Because of that, the diagrammatic expansion is more complicated in our case. Since the singularity occurs for any value of the spin, it is natural to group the diagrams by their order in $1/S$. By construction, the three-particle vertex is of order $1/\sqrt{S}$ relative to the magnon energy $\varepsilon_{\mathbf{k}}$ and it must occur in pairs in any self-energy diagram, while the four-particle vertex is of order $1/S$. We depict schematically all topologically different diagrams of orders $1/S$ and $1/S^2$ that occur in such a theory in Figs. 18(a)–18(d), respectively.

The singularity in our case is due to the "bubble" diagram [left in Fig. 18(a)], which leads to the logarithmic term for certain $\mathbf{k}$ values of external lines of the diagram. A simple

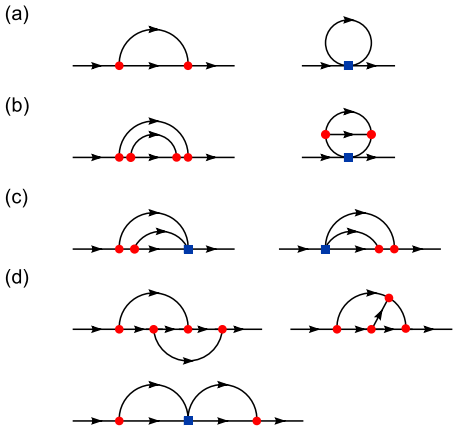

FIG. 18. (Color online) Schematic picture of all topologically inequivalent diagrams of order (a) $1/S$ and (b)–(d) $1/S^2$, respectively. The leading divergence in $1/S$ diagrams is $\ln|\Delta\omega|$ [first diagram in (a)] and in $1/S^2$ order it is $(\ln|\Delta\omega|)^2$ [all diagrams in (d)]. First two diagrams in (d) are identical.

analysis shows that out of the $1/S^2$ terms only diagrams in Fig. 18(d) yield the higher power of the log, $(\ln|\Delta\omega|)^2$. In fact, the first two diagrams in the (d) group are identical and can be seen as vertex corrections to the bubble in Fig. 18(a). The last diagram in the group (d) is the standard "two-bubble" member of the ladder sequence considered by Pitaevskii. A closer inspection of the second diagram in the (d) group in Fig. 18 makes it clear that it is also the "two-bubble" diagram with the virtual magnon line and two three-magnon vertices joining the bubbles. This modifies consideration by Pitaevskii, albeit only quantitatively, as it introduces extra interaction together with some retardation into the "ladder" sequence. To rule out the presence of any "nonladder"-type diagrams with the higher powers of the log and, hence, to eliminate the possibility of more complicated form of the nonanalytic behavior, the following observation is useful. In the parquet consideration,[54] it is both particle-particle and particle-hole diagrams that are singular. In our case of bosons with nonconserved number of particles at $T=0$, the particle-hole diagrams are all identically zero. Thus, the leading power of the log of any given diagram is simply the number of nonequivalent regions of the diagram in which a vertical cut intersects only two magnon lines. Therefore, the most-divergent diagram sequence is comprised of the ladderlike diagrams only, with both V_4 and $(V_3)^2$ between the bubbles. This can be confirmed by an explicit analysis of the "dangerous" diagrams in the next $1/S^3$ order (not shown in Fig. 18).

Another qualitative difference of our problem from the fermionic case in which the "parquet" summation is successful is that the latter consideration often exploits the long-wavelength character of the problem to obtain a universal answer. In our case, the singularity occurs at short wavelength. Therefore, even in the hypothetical generalization of our problem to the bosons with conserved number of particles and singular particle-hole bubbles, the parquetlike analysis is unlikely to be successful as the coefficients of the leading log powers will be independent from each other.

Altogether, presented analysis of higher-order divergences in the diagrammatic sequence for the magnon propagator in the noncollinear AFs shows that the singularities are regularized by summation of the ladder diagrams of the Pitaevskii type with the minor modification of the interaction vertex. The regularized result can be written schematically as

$$\Sigma \propto \frac{V_3^2\Pi}{1-\tilde{V}\Pi} \propto A + \frac{B}{\Pi} + \cdots, \tag{C1}$$

where $\tilde{V}=V_4+V_3GV_3$ and Π is the singular bubble contribution $(\sim\ln|\Delta\omega|)$.

APPENDIX D: OFF-SHELL DYSON EQUATION FOR COMPLEX ENERGIES

Suppose that the Dyson equation

$$\omega - \omega_{\mathbf{k}} - \Sigma(\mathbf{k},\omega) = 0 \tag{D1}$$

has a solution at a complex energy

$$\omega = \tilde{\omega}_{\mathbf{k}} - i\Gamma_{\mathbf{k}}, \quad \Gamma_{\mathbf{k}} > 0, \tag{D2}$$

where the sign of the imaginary part is dictated by causality. The Dyson equation can be written for the real and imaginary parts as

$$\tilde{\omega}_{\mathbf{k}} = \omega_{\mathbf{k}} + \mathrm{Re}[\Sigma(\mathbf{k},\tilde{\omega}_{\mathbf{k}} - i\Gamma_{\mathbf{k}})], \tag{D3}$$

$$\Gamma_{\mathbf{k}} = -\mathrm{Im}[\Sigma(\mathbf{k},\tilde{\omega}_{\mathbf{k}} - i\Gamma_{\mathbf{k}})] > 0. \tag{D4}$$

In the standard textbook approach[54] the damping is assumed to be small, $\Gamma_{\mathbf{k}} \ll \tilde{\omega}_{\mathbf{k}}$, and is neglected from the self-energy in the right-hand side of Eqs. (D3) and (D4). In that case, only the real part of the Dyson equation needs to be solved self-consistently while the damping is simply evaluated from the imaginary part of the self-energy at the real $\omega=\tilde{\omega}_{\mathbf{k}}$, which is the solution of Eq. (D3).

Since we have encountered a problem in which the imaginary part of the self-energy diverges at some $\mathbf{k}$ values for ω along the real axis, we would like to deviate from the standard approach and keep finite $\Gamma_{\mathbf{k}}$ in both parts of the Dyson equation, solving them self-consistently for both $\tilde{\omega}_{\mathbf{k}}$ and $\Gamma_{\mathbf{k}}$. However, on this path one discovers a difficulty that is unrelated to the singularity and is much more generic. We believe that it deserves a separate discussion.

Let us consider the self-energy of very general form

$$\Sigma(\mathbf{k},\omega) = \sum_{\mathbf{q}} \frac{|V_{\mathbf{k},\mathbf{q}}|^2}{\omega - \varepsilon_{\mathbf{q}} - \varepsilon_{\mathbf{k}-\mathbf{q}} + i0}. \tag{D5}$$

The self-energy of such type appears in the problem of phonon interaction with electron-hole continuum, Cherenkov radiation, or pair production in QED to name a few. All of these problems involve a (virtual) decay of a particle into two other particles. For simplicity, the products of the decay are assumed to be free particles (no damping for $\varepsilon_{\mathbf{q}}$'s). The difficulty arises when substituting $\omega=\tilde{\omega}_{\mathbf{k}}-i\Gamma_{\mathbf{k}}$ in the denominator of Eq. (D5). This shifts the pole in Eq. (D1) into the wrong (upper) ω half plane making $\Gamma_{\mathbf{k}}<0$, which violates causality and renders the Dyson equation unsolvable.

The resolution of this problem within the formalism of causal diagram technique requires one to define properly the

energy conservation for particles with finite lifetime. The self-energy (D5) is the result of integrating the bubblelike diagram over the internal frequency. Specifically, assuming for simplicity that the decay is into particles of the same species, one can write

$$\Sigma(\mathbf{k},\omega) = i\sum_{\mathbf{q}} \int_{\varepsilon} \frac{|V_{\mathbf{k},\mathbf{q}}|^2}{(\omega - \varepsilon - \varepsilon_{\mathbf{k}-\mathbf{q}} + i0)(\varepsilon - \varepsilon_{\mathbf{q}} + i0)}, \tag{D6}$$

where $\int_{\varepsilon} \equiv \int d\varepsilon/2\pi$. This step seems to make the problem even worse: substituting $\omega = \tilde{\omega}_{\mathbf{k}} - i\Gamma_{\mathbf{k}}$ in Eq. (D6) shifts the pole of the first Green's function into the wrong half plane, which renders the integral over internal frequency zero.

Making one more step back we recall that Eq. (D6) comes from the standard diagrammatic expression that explicitly reflects the conservation of energy within the decay process

$$\Sigma(\mathbf{k},\omega) = i\sum_{\mathbf{q}} \int_{\varepsilon} \int_{\varepsilon_1} \frac{|V_{\mathbf{k},\mathbf{q}}|^2 \delta(\omega - \varepsilon_1 - \varepsilon)}{(\varepsilon_1 - \varepsilon_{\mathbf{k}-\mathbf{q}} + i0)(\varepsilon - \varepsilon_{\mathbf{q}} + i0)}. \tag{D7}$$

Integrating Eq. (D7) over ε_1 gives Eq. (D6). Now, the only place where "external" energy ω enters the self-energy is the δ function. Thus, one needs to generalize the δ function in Eq. (D7) for the case when ω turns complex. An obvious trick is to represent the δ function by the Lorentzian of width $\Gamma_{\mathbf{k}}$. Then one can rewrite $\Sigma(\mathbf{k},\omega)$ for $\omega = \tilde{\omega}_{\mathbf{k}} - i\Gamma_{\mathbf{k}}$ as

$$\Sigma(\mathbf{k},\omega) = i\sum_{\mathbf{q}} \int_{\varepsilon} \int_{\varepsilon_1} \frac{|V_{\mathbf{k},\mathbf{q}}|^2 2\Gamma_{\mathbf{k}}}{(\tilde{\omega}_{\mathbf{k}} - \varepsilon_1 - \varepsilon)^2 + \Gamma_{\mathbf{k}}^2} \times \frac{1}{(\varepsilon_1 - \varepsilon_{\mathbf{k}-\mathbf{q}} + i0)(\varepsilon - \varepsilon_{\mathbf{q}} + i0)}. \tag{D8}$$

Note, that the above expression *does* respect the causality. Integrating it by standard means we obtain the desired well-behaved result

$$\Sigma(\mathbf{k},\omega) = \sum_{\mathbf{q}} \frac{|V_{\mathbf{k},\mathbf{q}}|^2}{\tilde{\omega}_{\mathbf{k}} - \varepsilon_{\mathbf{q}} - \varepsilon_{\mathbf{k}-\mathbf{q}} + i\Gamma_{\mathbf{k}}}. \tag{D9}$$

One can see that starting from the basic diagrammatic rules we obtain the result for the self-energy with the "wrong" sign of the imaginary part of the energy of the decaying particle. This resolves the problem. In the form (D9) the self-energy has the quasiparticle pole in the correct (lower) half plane and yields the correct sign of $\Gamma_{\mathbf{k}}$ in the Dyson equation. Thus, the prescription is: the energy of the decaying particle in the self-energy (D5) should be taken from the advanced Green's function. The "proper" Dyson equation then reads as

$$\omega - \omega_{\mathbf{k}} - \Sigma(\mathbf{k},\omega^*) = 0 \tag{D10}$$

for complex $\omega = \tilde{\omega}_{\mathbf{k}} - i\Gamma_{\mathbf{k}}$.

Using the Matsubara technique, the problem is resolved without any tricks with the δ function, but simply by forcing all the poles to be in the correct half plane. This does not give any additional insight, but means that the retarded self-energy simply corresponds to the complex conjugation of ω: $\Sigma_{\text{ret}}(\mathbf{k}, \tilde{\omega}_{\mathbf{k}} - i\Gamma_{\mathbf{k}}) \equiv \Sigma(\mathbf{k}, \tilde{\omega}_{\mathbf{k}} + i\Gamma_{\mathbf{k}})$. Thus, one can write the Dyson equation in an explicitly self-consistent form as

$$\tilde{\omega}_{\mathbf{k}} - i\Gamma_{\mathbf{k}} - \omega_{\mathbf{k}} - \Sigma(\mathbf{k}, \tilde{\omega}_{\mathbf{k}} + i\Gamma_{\mathbf{k}}) = 0, \tag{D11}$$

with $\Sigma(\mathbf{k},\omega)$ from Eq. (D5). Changing $\Gamma_{\mathbf{k}}$ to an infinitesimal δ, this expression is nothing but the standard Dyson equation obtained from the Matsubara approach [see Eqs. (3.140)–(3.142) of Ref. 54].

APPENDIX E: QUASIPARTICLE RESIDUE

Here we discuss an extension of the definition of the quasiparticle residue to the case of a particle with a finite lifetime. The concept of the quasiparticle residue is introduced in the context of the problem of interacting particles where it is assumed that after "dressing" the Green's function retains a well-defined pole at low energy. Close to that pole one can write the Green's function in the main-pole approximation

$$G_{\mathbf{k}}(\omega) \approx \frac{Z_{\mathbf{k}}}{\omega - \tilde{\omega}_{\mathbf{k}} + i0} + G_{\mathbf{k}}^{\text{incoh}}(\omega), \tag{E1}$$

where the incoherent part of the Green's function $G_{\mathbf{k}}^{\text{incoh}}(\omega)$ is regular at the "new" quasiparticle energy $\omega = \tilde{\omega}_{\mathbf{k}}$ and $Z_{\mathbf{k}}$ is the quasiparticle residue, $Z_{\mathbf{k}} < 1$. $Z_{\mathbf{k}}$ is also the weight associated with the δ-functional peak of the Green's function at $\omega = \tilde{\omega}_{\mathbf{k}}$. We wish to extend this to the case when the quasiparticle has a finite lifetime. In other words, we hope to be able to write

$$G_{\mathbf{k}}(\omega) = \frac{1}{\omega - \omega_{\mathbf{k}} - \Sigma_{\mathbf{k}}(\omega)} \approx \frac{Z_{\mathbf{k}}}{\omega - \tilde{\omega}_{\mathbf{k}} + i\Gamma_{\mathbf{k}}} + G_{\mathbf{k}}^{\text{incoh}}(\omega). \tag{E2}$$

To get from the left-hand side to the right-hand side we need to assume that there exist a solution of the Dyson equation

$$\omega - \omega_{\mathbf{k}} - \Sigma_{\mathbf{k}}(\omega) = 0 \tag{E3}$$

at some complex $\omega = \tilde{\omega}_{\mathbf{k}} - i\Gamma_{\mathbf{k}}$, where

$$\tilde{\omega}_{\mathbf{k}} = \omega_{\mathbf{k}} + \text{Re}[\Sigma_{\mathbf{k}}(\tilde{\omega}_{\mathbf{k}} - i\Gamma_{\mathbf{k}})], \tag{E4}$$

$$\Gamma_{\mathbf{k}} = -\text{Im}[\Sigma_{\mathbf{k}}(\tilde{\omega}_{\mathbf{k}} - i\Gamma_{\mathbf{k}})]. \tag{E5}$$

Then, as in the standard approach, we proceed by adding and subtracting $\Sigma_{\mathbf{k}}(\tilde{\omega}_{\mathbf{k}} - i\Gamma_{\mathbf{k}}) = \tilde{\omega}_{\mathbf{k}} - \omega_{\mathbf{k}} - i\Gamma_{\mathbf{k}}$ to the denominator of $G_{\mathbf{k}}(\omega)$,

$$G_{\mathbf{k}}(\omega) = \frac{1}{\omega - \omega_{\mathbf{k}} - \Sigma_{\mathbf{k}}(\omega)} = \frac{1}{\omega - \tilde{\omega}_{\mathbf{k}} + i\Gamma_{\mathbf{k}} - [\Sigma_{\mathbf{k}}(\omega) - \Sigma_{\mathbf{k}}(\tilde{\omega}_{\mathbf{k}} - i\Gamma_{\mathbf{k}})]}. \tag{E6}$$

This can be rewritten without approximation as

$$G_{\mathbf{k}}(\omega) \equiv \frac{1}{\omega - \tilde{\omega}_{\mathbf{k}} + i\Gamma_{\mathbf{k}}} \left[1 - \left(\frac{\Sigma_{\mathbf{k}}(\omega) - \Sigma_{\mathbf{k}}(\tilde{\omega}_{\mathbf{k}} - i\Gamma_{\mathbf{k}})}{\omega - \tilde{\omega}_{\mathbf{k}} + i\Gamma_{\mathbf{k}}} \right) \right]^{-1}. \tag{E7}$$

Near the pole, $\omega \to \tilde{\omega}_{\mathbf{k}} - i\Gamma_{\mathbf{k}}$, this expression finally yields

$$G_{\mathbf{k}}(\omega) \approx \frac{Z_{\mathbf{k}}}{\omega - \tilde{\omega}_{\mathbf{k}} + i\Gamma_{\mathbf{k}}}, \tag{E8}$$

where

$$Z_{\mathbf{k}} \equiv \left[1 - \left.\frac{\partial \Sigma_{\mathbf{k}}(\omega)}{\partial \omega}\right|_{\omega=\tilde{\omega}_{\mathbf{k}}-i\Gamma_{\mathbf{k}}}\right]^{-1}, \tag{E9}$$

which coincides with the standard definition of $Z_{\mathbf{k}}$ up to the change of $\tilde{\omega}_{\mathbf{k}}$ to $\tilde{\omega}_{\mathbf{k}} - i\Gamma_{\mathbf{k}}$.[54] Therefore, generally speaking, the quasiparticle residue obtained this way is complex. However, one would prefer to have $Z_{\mathbf{k}}$ real in accord with the expectation that the area under the Lorentzian (broadened δ peak) should give the quasiparticle weight. For that, let us consider the spectral function

$$A_{\mathbf{k}}(\omega) = \frac{1}{\pi}\left(\frac{\Gamma_{\mathbf{k}}\,\mathrm{Re}[Z_{\mathbf{k}}]}{(\omega - \tilde{\omega}_{\mathbf{k}})^2 + \Gamma_{\mathbf{k}}^2} - \frac{(\omega - \tilde{\omega}_{\mathbf{k}})\mathrm{Im}[Z_{\mathbf{k}}]}{(\omega - \tilde{\omega}_{\mathbf{k}})^2 + \Gamma_{\mathbf{k}}^2}\right), \tag{E10}$$

where the first term has the Lorentzian form while the second one vanishes at $\omega_{\mathbf{k}} = \tilde{\omega}_{\mathbf{k}}$. Clearly, the second part of the expression is odd in ω and the spectral weight of the quasiparticle peak, which is given by the integral of $A_{\mathbf{k}}(\omega)$ along the real axis,

$$\int_{-\infty}^{\infty} A_{\mathbf{k}}(\omega) d\omega \equiv \mathrm{Re}[Z_{\mathbf{k}}], \tag{E11}$$

is simply the real part of $Z_{\mathbf{k}}$ in Eq. (E9). This gives a proper definition of the "generalized" quasiparticle residue

$$Z_{\mathbf{k}} \equiv \mathrm{Re}\left(\left[1 - \left.\frac{\partial \Sigma_{\mathbf{k}}(\omega)}{\partial \omega}\right|_{\omega=\tilde{\omega}_{\mathbf{k}}-i\Gamma_{\mathbf{k}}}\right]^{-1}\right). \tag{E12}$$

Interestingly, this definition differs from the one in Ref. 54.

Our interest in this problem is twofold. First, we deal with quasiparticles that have finite damping due to decays. Second, the decay part of the self-energy, Eq. (33), near the log singularity has derivatives that are even more singular. In particular, an attempt to calculate the quasiparticle residue using the on-shell approach near the saddle-point singularity $\mathbf{k} \to \mathbf{k}^*$ leads to

$$\left.\frac{\partial \Sigma_{11}^{(a)}(\mathbf{k},\omega)}{\partial \omega}\right|_{\omega_{\mathbf{k}}} = -\frac{1}{2}\sum_{\mathbf{q}} \frac{\tilde{\Gamma}_1(\mathbf{q};\mathbf{k})^2}{(\omega_{\mathbf{k}} - \omega_{\mathbf{q}} - \omega_{\mathbf{k}-\mathbf{q}} + i0)^2},$$

whose imaginary part is divergent as $\propto (k-k^*)^{-1}$ and the real part has a δ-function singularity at $k=k^*$. If, on the other hand, one uses the solution of the Dyson equation together with our more general definition of $Z_{\mathbf{k}}$ [Eq. (E12)], the result becomes regular. This is yet another way of saying that the $1/S$ expansion in the noncollinear AFs is singular and the usual on-shell approach cannot be used.

Interestingly, the off-shell consideration gives, after some algebra, that in the large-S limit, at the singular $\mathbf{k}$ points $(\partial\Sigma/\partial\omega) \propto 1/\ln S$. This means that the quasiparticle residue reaches the classical limit (=1) very slowly as

$$Z_{\mathbf{k}} \approx \left(1 - \frac{A}{\ln S}\right)^{-1}$$

at these points.

[1] Review of early works is given by M. F. Collins and O. A. Petrenko, Can. J. Phys. **75**, 605 (1997).

[2] R. Coldea, D. A. Tennant, A. M. Tsvelik, and Z. Tylczynski, Phys. Rev. Lett. **86**, 1335 (2001); R. Coldea, D. A. Tennant, K. Habicht, P. Smeibidl, C. Wolters, and Z. Tylczynski, *ibid.* **88**, 137203 (2002).

[3] L. E. Svistov, A. I. Smirnov, L. A. Prozorova, O. A. Petrenko, L. N. Demianets, and A. Ya. Shapiro, Phys. Rev. B **67**, 094434 (2003).

[4] S. Nakatsuji, Y. Nambu, H. Tonomura, O. Sakai, S. Jonas, C. Broholm, H. Tsunetsugu, Y. Qiu, and Y. Maeno, Science **309**, 1697 (2005).

[5] A. Olariu, P. Mendels, F. Bert, B. G. Ueland, P. Schiffer, R. F. Berger, and R. J. Cava, Phys. Rev. Lett. **97**, 167203 (2006).

[6] D. Hsieh, D. Qian, R. F. Berger, R. J. Cava, J. W. Lynn, Q. Huang, and M. Z. Hasan, J. Phys. Chem. Solids **69**, 3174 (2008); Physica B **403**, 1341 (2008).

[7] P. W. Anderson, Mater. Res. Bull. **8**, 153 (1973); P. Fazekas and P. W. Anderson, Philos. Mag. **30**, 423 (1974).

[8] T. Oguchi, J. Phys. Soc. Jpn. Suppl. **52**, 183 (1983).

[9] Th. Jolicoeur and J. C. Le Guillou, Phys. Rev. B **40**, 2727 (1989).

[10] S. J. Miyake, J. Phys. Soc. Jpn. **61**, 983 (1992).

[11] A. V. Chubukov, S. Sachdev, and T. Senthil, J. Phys.: Condens. Matter **6**, 8891 (1994).

[12] P. W. Leung and K. J. Runge, Phys. Rev. B **47**, 5861 (1993).

[13] B. Bernu, P. Lecheminant, C. Lhuillier, and L. Pierre, Phys. Rev. B **50**, 10048 (1994).

[14] L. Capriotti, A. E. Trumper, and S. Sorella, Phys. Rev. Lett. **82**, 3899 (1999).

[15] W. H. Zheng, J. O. Fjærestad, R. R. P. Singh, R. H. McKenzie, and R. Coldea, Phys. Rev. B **74**, 224420 (2006).

[16] S. R. White and A. L. Chernyshev, Phys. Rev. Lett. **99**, 127004 (2007).

[17] N. Elstner, R. R. P. Singh, and A. P. Young, Phys. Rev. Lett. **71**, 1629 (1993); N. Elstner, R. R. P. Singh, and A. P. Young, J. Appl. Phys. **75**, 5943 (1994).

[18] W. Zheng, J. O. Fjærestad, R. R. P. Singh, R. H. McKenzie, and R. Coldea, Phys. Rev. Lett. **96**, 057201 (2006).

[19] O. A. Starykh, A. V. Chubukov, and A. G. Abanov, Phys. Rev. B **74**, 180403(R) (2006).

[20] A. L. Chernyshev and M. E. Zhitomirsky, Phys. Rev. Lett. **97**, 207202 (2006).

[21] Zheng Weihong, J. Oitmaa, and C. J. Hamer, Phys. Rev. B **43**, 8321 (1991).

[22] A. W. Sandvik, Phys. Rev. B **56**, 11678 (1997).

[23] A. W. Sandvik and R. R. P. Singh, Phys. Rev. Lett. **86**, 528 (2001).

[24] W. Zheng, J. Oitmaa, and C. J. Hamer, Phys. Rev. B **71**, 184440 (2005).
[25] F. J. Dyson, Phys. Rev. **102**, 1217 (1956).
[26] T. Oguchi, Phys. Rev. **117**, 117 (1960).
[27] A. B. Harris, D. Kumar, B. I. Halperin, and P. C. Hohenberg, Phys. Rev. B **3**, 961 (1971).
[28] J. M. Ziman, *Electrons and phonons* (Oxford University Press, New York, 1960).
[29] E. M. Lifshits and L. P. Pitaevskii, *Statistical Physics II* (Pergamon, New York, 1980).
[30] M. E. Zhitomirsky, Phys. Rev. B **73**, 100404(R) (2006).
[31] M. B. Stone, I. A. Zaliznyak, T. Hong, D. H. Reich, and C. L. Broholm, Nature (London) **440**, 187 (2006).
[32] S. J. Miyake, Prog. Theor. Phys. **74**, 468 (1985).
[33] T. Ohyama and H. Shiba, J. Phys. Soc. Jpn. **62**, 3277 (1993).
[34] M. E. Zhitomirsky and T. Nikuni, Phys. Rev. B **57**, 5013 (1998).
[35] N. Perkins and W. Brenig, Phys. Rev. B **77**, 174412 (2008).
[36] M. E. Zhitomirsky and A. L. Chernyshev, Phys. Rev. Lett. **82**, 4536 (1999).
[37] O. F. Syljuasen, Phys. Rev. B **78**, 180413(R) (2008).
[38] A. Luscher and A. Laeuchli, arXiv:0812.3420, Phys. Rev. B (to be published).
[39] T. Dombre and N. Read, Phys. Rev. B **39**, 6797 (1989).
[40] M. Y. Veillette, A. J. A. James, and F. H. L. Essler, Phys. Rev. B **72**, 134429 (2005).
[41] D. Dalidovich, R. Sknepnek, A. J. Berlinsky, J. Zhang, and C. Kallin, Phys. Rev. B **73**, 184403 (2006).
[42] A. Kreisel, F. Sauli, N. Hasselmann, and P. Kopietz, Phys. Rev. B **78**, 035127 (2008).
[43] H. Neuberger and T. Ziman, Phys. Rev. B **39**, 2608 (1989).
[44] S. T. Beliaev, Sov. Phys. JETP **7**, 299 (1958).
[45] L. P. Pitaevskii and Y. B. Levinson, Phys. Rev. B **14**, 263 (1976).
[46] L. P. Pitaevskii, Zh. Eksp. Teor. Fiz. **36**, 1168 (1959) [Sov. Phys. JETP **9**, 830 (1959)].
[47] H. Tsujii, C. R. Rotundu, T. Ono, H. Tanaka, B. Andraka, K. Ingersent, and Y. Takano, Phys. Rev. B **76**, 060406(R) (2007).
[48] M. Bocquet, F. H. L. Essler, A. M. Tsvelik, and A. O. Gogolin, Phys. Rev. B **64**, 094425 (2001).
[49] M. Kohno, O. A. Starykh, and L. Balents, Nat. Phys. **3**, 790 (2007).
[50] J. T. Chalker, P. C. W. Holdsworth, and E. F. Shender, Phys. Rev. Lett. **68**, 855 (1992).
[51] A. B. Harris, C. Kallin, and A. J. Berlinsky, Phys. Rev. B **45**, 2899 (1992).
[52] A. Chubukov, Phys. Rev. Lett. **69**, 832 (1992).
[53] K. Matan, D. Grohol, D. G. Nocera, T. Yildirim, A. B. Harris, S. H. Lee, S. E. Nagler, and Y. S. Lee, Phys. Rev. Lett. **96**, 247201 (2006).
[54] G. D. Mahan, *Many-Particle Physics*, 3rd ed. (Plenum, New York, 2000).
[55] T. Giamarchi, *Quantum Physics in One Dimension* (Oxford University Press, New York, 2003).
[56] A. H. Castro Neto, F. Guinea, N. M. R. Peres, K. S. Novoselov, and A. K. Geim, Rev. Mod. Phys. **81**, 109 (2009).
[57] S. P. Bayrakci, T. Keller, K. Habicht, and B. Keimer, Science **312**, 1926 (2006).
[58] O. F. Syljuasen and P. A. Lee, Phys. Rev. Lett. **88**, 207207 (2002).